

1 **Atmospherically-forced sea-level variability in western Hudson Bay, Canada**

2
3 Igor A. Dmitrenko^{1,*}, Denis L. Volkov^{2,3}, Tricia A. Stadnyk⁴, Andrew Tefs⁴, David G. Babb¹,
4 Sergey A. Kirillov¹, Alex Crawford¹, Kevin Sydor⁵, and David G. Barber¹

5
6
7 ¹Centre for Earth Observation Science, University of Manitoba, Winnipeg, Manitoba, Canada

8 ²Cooperative Institute for Marine and Atmospheric Studies, University of Miami, Miami,
9 Florida, USA

10 ³NOAA, Atlantic Oceanographic and Meteorological Laboratory, Miami, Florida, USA

11 ⁴Department of Geography, University of Calgary, Calgary, Alberta, Canada

12 ⁵Manitoba Hydro, Winnipeg, Manitoba, Canada

13
14
15
16
17
18
19
20
21
22
23
24
25
26
27
28 *Corresponding author, igor.dmitrenko@umanitoba.ca, 125 Dysart Rd., University of Manitoba,
29 Winnipeg, Manitoba R3T 2N2 Canada

30 **Abstract:** In recent years, significant trends toward earlier breakup and later freeze-up of sea-ice
31 in Hudson Bay have led to a considerable increase in shipping activity through the Port of
32 Churchill, which is located in western Hudson Bay and is the only deep-water ocean port in the
33 province of Manitoba. Therefore, understanding sea-level variability at the Port is an urgent
34 issue crucial for safe navigation and coastal infrastructure. Using tidal gauge data from the Port
35 along with an atmospheric reanalysis and Churchill River discharge, we assess environmental
36 factors impacting synoptic to seasonal variability of sea-level at Churchill. An atmospheric
37 vorticity index used to describe the wind forcing was found to correlate with sea level at
38 Churchill. Statistical analyses show that, in contrast to earlier studies, local discharge from the
39 Churchill River can only explain up to 5% of the sea level variability. The cyclonic wind forcing
40 contributes from 22% during the ice-covered winter-spring season to 30% during the ice-free
41 summer-fall season due to cyclone-induced storm surge generated along the coast. Multiple
42 regression analysis revealed that wind forcing and local river discharge combined can explain up
43 to 32% of the sea level variability at Churchill. Our analysis further revealed that the seasonal
44 cycle of sea level at Churchill appears to be impacted by the seasonal cycle in atmospheric
45 circulation rather than by the seasonal cycle in local discharge from the Churchill River,
46 particularly post-construction of the Churchill River diversion in 1977. Sea level at Churchill
47 shows positive anomalies for September-November compared to June-August. This seasonal
48 difference was also revealed for the entire Hudson Bay coast using satellite-derived sea level
49 altimetry. This anomaly was associated with enhanced cyclonic atmospheric circulation during
50 fall, reaching a maximum in November, which forced storm surges along the coast. Complete
51 sea-ice cover during winter impedes momentum transfer from wind stress to the water column,
52 reducing the impact of wind forcing on sea level variability. Expanding our observations to the
53 bay-wide scale, we confirmed the process of wind-driven sea-level variability with (i) tidal-
54 gauge data from eastern Hudson Bay and (ii) satellite altimetry measurements. Ultimately, we
55 find that cyclonic winds generate sea level rise along the western and eastern coasts of Hudson
56 Bay at the synoptic and seasonal time scales, suggesting an amplification of the bay-wide
57 cyclonic geostrophic circulation in fall (October-November), when cyclonic vorticity is
58 enhanced, and Hudson Bay is ice-free.

59 **Keywords:** Hudson Bay; sea level; Churchill River discharge; atmospheric vorticity.

60

61 1. Introduction

62 Hudson Bay in northeast Canada is a shallow (mean depth ~ 150 m), semi-enclosed sub-arctic
63 inland sea that is connected to the Labrador Sea through Hudson Strait (Figure 1). The Bay
64 occupies approximately 831,000 km², making it the world's largest inland sea, and is
65 characterized by a high annual volume of river discharge (712 km³; Déry *et al.*, 2005; 2011) and
66 a dynamic seasonal ice cover that exists from November/December to June/July (Hochheim and
67 Barber, 2010; 2014). The mean circulation in Hudson Bay is comprised of the wind-driven and
68 estuarine components, where the estuarine portion is driven by the riverine water input
69 (Prinsenber, 1986a), and the wind-driven portion is attributed to Pprevailing along-
70 shoreeyelonic winds drive cyclonic circulation of water within the Bay (e.g., Ingram and

71 *Prinsenber*, 1998; *Saucier et al.*, 2004; *St-Laurent et al.*, 2011; *Ridenour et al.*, 2019a;
72 *Dmitrenko et al.*, 2020). Model simulations by *Saucier et al.* (2004) show that the cyclonic
73 circulation is stronger during fall, reaching a maximum in November when the winds are
74 strongest, and weakest in spring when Hudson Bay has a complete sea-ice cover. *Dmitrenko et*
75 *al.* (2020), however, found that even during the ice covered season strong cyclones can amplify
76 ~~eyelonic~~ water circulation in the Bay. This is consistent with conclusions by *St-Laurent et al.*
77 (2011), who noted that momentum is transmitted through the mobile ice pack to the water
78 column. The efficiency of momentum transmission through the mobile ice strongly depends on
79 sea-ice roughness, which is impacted by ice concentration and characteristic length scales of
80 roughness elements including pressure ridges, melt ponds etc. (e.g., *Lüpkes et al.*, 2012;
81 *Tsamados et al.*, 2014; *Joyce et al.*, 2019). In particular, ice floes in a state of free drift within a
82 partial or weak ice cover, typical of the polynya area in western Hudson Bay, increase the
83 transfer of wind stress into the water column (*Schulze and Pickart*, 2012). Both velocity
84 measurements (*Prinsenber*, 1986b; *Ingram and Prinsenber*, 1998; *Dmitrenko et al.*, 2020) and
85 model simulations (*Wang et al.*, 1994; *Saucier et al.*, 2004; *St-Laurent et al.*, 2011; *Ridenour et*
86 *al.*, 2019b) show that during summer, cyclonic water circulation produces a ~~eyelonic~~-coastal
87 transport corridor that advects riverine water along the coast toward Hudson Strait and into the
88 Labrador Sea.

89 The local water mass of Hudson Bay is dominated by freshwater input comprised of river runoff
90 from the largest watershed in Canada and sea-ice meltwater (e.g., *Prinsenber*, 1984, 1988,
91 1991; *Saucier and Dionne*, 1998; *Granskog et al.*, 2009; *Eastwood et al.*, 2020). The annual
92 mean discharge rate of $22.6 \times 10^3 \text{ m}^3 \text{ s}^{-1}$ corresponds to a net discharge of 712 km^3 of freshwater
93 per year (*Déry et al.*, 2005, 2011). A similar volume of In April, about $742 \pm 10 \text{ km}^3$ of
94 freshwater ~~withdrawn from the surface water layer by ice growth~~ is contained within the ice pack
95 by April (*Landy et al.*, 2017). Freshwater transport in Hudson Bay exhibits a strong seasonal
96 cycle influenced by the timing of river discharge (e.g., *Déry et al.*, 2005), the annual melt/freeze
97 cycle of sea ice (*Ingram and Prinsenber*, 1998; *Saucier et al.*, 2004; *Straneo and Saucier*, 2008;
98 *Granskog et al.*, 2011), and seasonality of wind forcing (*Saucier et al.*, 2004; *St-Laurent et al.*,
99 2011).

100 During the last decade, significant progress has been achieved in understanding the Hudson Bay
101 environmental system (e.g., *Granskog et al.*, 2009; *Kuzyk et al.*, 2011; *St-Laurent et al.*, 2011;
102 *Piecuch and Ponte*, 2015; *Landy et al.*, 2017; *Kuzyk and Candlish*, 2019; *Eastwood et al.*, 2020;
103 *Dmitrenko et al.*, 2020, 2021). However, the synoptic, seasonal, and interannual variability of sea
104 level in Hudson Bay still remains insufficiently studied due to a scarcity of sea level observations
105 at permanent tidal gauges. Note that the tidal gauge in Churchill (Figure 1) is the only
106 continuously operating tide gauge in Hudson Bay and the central Canadian Arctic. Historically,
107 the focus of sea level studies in Hudson Bay was motivated by this area's post-glacial isostatic
108 rebound (e.g., *Guttenberg*, 1941; *Tushingham*, 1992); for a detailed review of these earlier
109 studies see *Wolf et al.* (2006). The advent of space-geodesy, in particular GPS, absolute-
110 gravimetry, and satellite altimetry measurements (e.g., *Larson and van Dam*, 2000; *Wolf et al.*,
111 2006; *Sella et al.*, 2007) afforded a shift in focus for Hudson Bay sea level research to
112 environmental aspects related to global warming and hydroelectric regulation (*Gough*, 1998,

113 2000), and those associated with increasing the shipping traffic from the Port of Churchill
114 through Hudson Bay to Hudson Strait, which may soon become a federally-designated
115 transportation corridor (e.g., *Andrews et al.*, 2017; *Pew Charitable Trusts*, 2016).

116 In 2016, the University of Manitoba and Manitoba Hydro launched a project on “Variability and
117 change of freshwater-marine coupling in the Hudson Bay System”, named BaySys, which aimed
118 to assess the relative contributions of climate change and river regulation to the Hudson Bay
119 system. Here, we are specifically focused on the impact of the Churchill River diversion on
120 variability of sea level at the Port of Churchill. Additionally, we put our findings in the context of
121 wind forcing over the entire Hudson Bay, elaborating on the suggestion by *Dmitrenko et al.*
122 (2020) that cyclonic wind forcing generates onshore Ekman transport and storm surges along the
123 coast.

124 We also revisit earlier results by *Gough and Robinson* (2000) and *Gough et al.* (2005). Using
125 tidal gauge and river discharge data from 1974 to 1994, *Gough and Robinson* (2000) suggested
126 that the Churchill River discharge dominates sea-level variability at Churchill. They explained
127 the seasonal elevation of sea level during late fall by a recirculating mechanism that links the
128 spring pulse of river discharge in the downstream James Bay (Figure 1) to sea level at Churchill
129 (*Gough and Robinson*, 2000; *Gough et al.*, 2005). In this paper, we present an alternative
130 mechanism and show that (i) the Churchill River discharge plays a secondary role for generating
131 sea level anomalies at Churchill, and (ii) the synoptic and seasonal variability of sea level at
132 Churchill and over the entire Hudson Bay is impacted by the wind forcing described with an
133 atmospheric vorticity index (Figure 2).

134

135 **2. Data**

136 2.1. *Sea level*

137 The daily mean sea level data used in this study were retrieved from the Canadian Tides and
138 Water Levels Data Archive of the Fisheries and Oceans Canada through [http://www.isdm-
139 gdsi.gc.ca/isdm-gdsi/twl-mne/index-eng.htm#s5](http://www.isdm-gdsi.gc.ca/isdm-gdsi/twl-mne/index-eng.htm#s5) (last access: 26 August 2021). Measurements of
140 sea level at Churchill were obtained from the permanent tidal gauge that is installed at the port of
141 Churchill (station #5010) near the mouth of the Churchill River (Figure 1). ~~This is the only~~
142 ~~permanently operating tide gauge in Hudson Bay and the central Canadian Arctic.~~ While
143 measurements of sea level at Churchill date back to the 1930s (*Gutenberg*, 1941), we only used
144 data from 1950 to present (Figure 3a), which is coincident with atmospheric reanalysis data from
145 the National Centers for Environmental Prediction (NCEP; *Kalnay et al.*, 1996). In addition, we
146 used sea level data from the temporary tidal gauge in Inukjuak (station #4575), Cape Jones
147 Island (station #4656), and North Kopak Island (station #4548) (Figure 1). Among these three
148 locations, only data at Inukjuak are fully representative for our analysis because they span a
149 sufficiently long period from October 1969 to October 1980, however, only the portion of this
150 time series from September 1973 to December 1975 is continuous. Sea level records at Cape
151 Jones Island and North Kopak Island are from August-October 1973 and 1975, respectively, and

152 were selected among other temporary stations in Hudson Bay to overlap with sea level time
153 series at Innujuak.

154 Satellite altimetry data from 1993-2020 were used to analyze the relationship between wind
155 forcing and sea level changes over the entire Hudson Bay. We used the daily fields of absolute
156 dynamic topography (ADT), i.e. the sea surface height above geoid, processed and distributed by
157 Copernicus Marine and Environment Monitoring Service (CMEMS;
158 <https://marine.copernicus.eu/>; last access: 26 August 2021). The ADT is obtained by adding a
159 mean dynamic topography (DT2018, Mulet et al., 2013) to sea level anomaly (SLA) measured
160 by altimetry satellites. The CMEMS SLA/ADT fields are computed by optimally interpolating
161 using data from all satellites available at a given time following a methodology described in
162 Pujol et al. (2016). Prior to mapping, altimetry records are corrected for instrumental noise, orbit
163 determination error, atmospheric refraction, sea state bias, static and dynamic atmospheric
164 pressure effects, and tides. Because in this work we are interested in local (dynamic) changes of
165 sea level, the global mean sea level was subtracted from each ADT map. Then the seasonal
166 climatology was computed for July through August (JJA) and September through November
167 (SON) by averaging all available maps during the respective seasons. Sea ice does not represent
168 a significant problem for computing the climatology, because Hudson Bay is essentially ice free
169 during these months, especially during SON.

170 The root-mean-square differences between tide gauge records and collocated SLA/ADT data are
171 usually 3-5 cm (e.g., Volkov et al., 2007; Pascual et al., 2009; Volkov et al., 2012) and do not
172 exceed 10 cm globally (CLS-DOS, 2016). When the altimetry data are averaged to produce the
173 seasonal climatology, the measurement error is greatly reduced (at least by an order of
174 magnitude for 28 years of altimetry record). It should be noted that altimetry errors near the coast
175 are greater than in the open ocean. This is due to land contamination within the radar footprint
176 and to the fact that the geophysical corrections applied to altimetry data are usually optimized for
177 the open ocean and not for the coastal zones. In classical altimetry products, however, a large
178 percentage of data within 10–15 km from the coast is deemed invalid and not used for generating
179 SLA/ADT maps (e.g., The Climate Change Initiative Coastal Sea Level Team, 2020).
180 Furthermore, satellite altimetry data was used here only for a qualitative assessment of the basin-
181 scale seasonal sea-level patterns in Hudson Bay. Therefore, the reduced quality of altimetry
182 retrievals near the coast is not expected to impact the conclusions of this study. Sea ice also does
183 not represent a significant problem for computing the climatology, because Hudson Bay is
184 essentially ice free during these months, especially during SON.

185 2.2. River discharge

186 Churchill River discharge data were obtained from Déry et al. (2016) and extended to 2019;
187 thus, we use a continuous record of daily mean discharge from 1960 to 2019 (Figure 4a and
188 supplementary material). The record was constructed from gauged observations above Red Head
189 Rapids (station #06FD001), which is located ~87 km from the Churchill River mouth and is the
190 most downstream hydrometric gauge along the Churchill River. When these data were not
191 available, we used upstream gauges (applying a drainage area correction) to fill significant gaps
192 in the time series (see Déry et al. 2005+6 for detailed methods). Data were adjusted by drainage

193 area (between the hydrometric gauge location and river outlet) and any significant tributary
194 inflows were added to represent discharge at the outlet of the Churchill River.

195 2.3. Wind forcing

196 Fields of sea level pressure (SLP) and 10-m wind velocity at 6-h intervals were derived from the
197 NCEP atmospheric reanalysis (<https://psl.noaa.gov/data/composites/hour/>; last access: 26 August
198 2021). We chose the NCEP reanalysis to extend the atmospheric forcing data back to 1950,
199 which covers the tide gauge record from Churchill, while a previous comparison of wind speeds
200 from NCEP and ERA5 (*Copernicus Climate Change Service*, 2017; *Hersbach et al.*, 2020) with
201 in situ observations from the Churchill weather station revealed an insignificant discrepancy
202 between the two reanalyses and meteorological observations (*Dmitrenko et al.*, 2020). However,
203 we used the ERA5 SLP data to validate atmospheric vorticity derived from NCEP as described
204 below in section 3. For simplicity, cyclones over the Hudson Bay area were manually tracked
205 for August-May 1969-1970 and 2003-2004 using the NCEP SLP fields, with the central position
206 and low SLP tabulated. The horizontal resolution of the NCEP-derived data is 2.5° of latitude
207 and longitude.

208 For the majority of tidal gauge data from 1950s, sea level at Churchill was recorded hourly. In
209 contrast, the Churchill River discharge from gauged observations above Red Head Rapids
210 (station #06FD001) is available daily. The NCEP data on SLP and 10-m wind are available at 6-
211 h intervals. To make these three time series comparable, we analyzed daily means.

212

213 3. Methods

214 For the 1950/60–2019 study period, a vorticity index was derived from the daily mean SLP
215 NCEP data to characterize the wind forcing and compare to the time series of sea level anomalies
216 (Figures 2a, 3a, and 4a). The vorticity index gives both the sign and magnitude of atmospheric
217 vorticity; it was first proposed by *Walsh et al.* (1996) and then successfully used for describing
218 atmospheric forcing over the Siberian shelves (*Dmitrenko et al.*, 2008a; 2008b) and Hudson Bay
219 (*Dmitrenko et al.*, 2020). The vorticity index is defined as the numerator of the finite difference
220 Laplacian of SLP for an area within a radius of 550 km centered at 60°N and 85°W in Hudson
221 Bay (Figure 1). A positive index corresponds to cyclonic atmospheric circulation that is typically
222 associated with northerly winds in western Hudson Bay, whereas a negative vorticity index
223 corresponds to anticyclonic atmospheric circulation characterized by southerly winds in western
224 Hudson Bay (Figure 2). *Dmitrenko et al.* (2020) examined the spatial uncertainty of atmospheric
225 vorticity estimated at 60°N, 85°W by computing vorticity for the 5-point stencils with a central
226 node shifted relative to 60°N, 85°W by approximately 280 km northward, eastward, southward,
227 and westward. Their results show that vorticity computed at 60°N, 85°W best describes major
228 cyclonic storms observed in 2016–2017.

229 The vorticity index used in this study does not fully explain the observed variability of
230 meridional wind in western Hudson Bay (Figure 2b), which is mainly responsible for generating
231 storm surge along the coast (*Dmitrenko et al.*, 2020). However, vorticity describes the intensity

232 of cyclonic wind forcing over the entire Bay impacting the basin-scale circulation and sea level
233 deformations along the entire coastline of Hudson Bay (Dmitrenko et al., 2020). Thus, our
234 approach allowed us to extend our findings over the entire Bay. We also conducted a validation
235 comparing the NCEP-derived vorticity to that derived from the ERA5 SLP utilizing the Web-
236 Based Reanalysis Intercomparison Tools (<https://psl.noaa.gov/cgi-bin/data/testdap/timeseries.pl>;
237 last access: 26 August 2021) described by Smith et al. (2014). The comparison showed
238 insignificant differences between the two reanalyses: the NCEP-derived vorticity only slightly
239 exceeds that obtained from ERA5, while the correlation between the NCEP and ERA5-derived
240 vorticities is 0.96 (Figure 2a).

241 The Churchill River discharge time series (Figure 4a) was compiled as follows. First, no
242 significant gaps in Churchill River discharge record occurred on a daily basis. There were,
243 however, some missing discharge data between 1976 and 1995, with some gaps up to 3 months
244 (e.g., 1984, 1987). When data gaps occurred, then the upstream hydrometric gauge below Fidler
245 Lake (station #06FB001) was used to infill data, with streamflow data adjusted to account for the
246 difference in contributing area between Fidler Lake and the Churchill outlet, following the
247 procedure of Déry et al. (2005). When the upstream hydrometric data were also unavailable, a
248 secondary step was taken to infill data gaps. Missing data on a given day were infilled using the
249 day-of-year mean value of streamflow over the available period of record. This procedure
250 constructed a daily climatology of streamflow (i.e., mean annual hydrograph) based on the
251 availability of data over the period of record.

252 For the Churchill River, however, we constructed a separate climatology of daily streamflow for
253 the periods prior to and after flow diversion in 1977. Partial diversion began in 1976, allowing
254 less than the full capacity of discharge to be diverted into the Nelson River system, with full
255 operation beginning in 1977. We therefore designated 1977 as the first year when diversion
256 became operational.

257 It is also important to separate the pre- and post-regulation periods for the analysis of the
258 potential impact natural (pre-diversion) and regulated Churchill River discharge have on sea
259 level anomalies at Churchill. Déry et al. (2016) reported that the Churchill River diversion
260 caused a significant decline in the mean annual discharge from $37.0 \pm 4.2 \text{ km}^3 \text{ year}^{-1}$ pre-
261 diversion (1964–73) compared to post-diversion flows (8.4 ± 2.9 and $9.6 \pm 4.4 \text{ km}^3 \text{ year}^{-1}$ for
262 1984–93 and 1994–2003, respectively). Déry et al. (2016) further revealed the coefficient of
263 variation (CV) of annual Churchill River discharge increased in inter-decadal CV post-diversion
264 (1984–2013; $\text{CV} = 0.35\text{--}0.67$) compared to pre-diversion records (1964–1973; $\text{CV} = 0.11$). Both
265 the decline in mean annual discharge and increase in discharge variability for the post-diversion
266 period necessitate separate analysis of the impact of river discharge on sea level variability due
267 to non-stationarity in the discharge record, which was implemented in our analysis.

268 The sea level record in Churchill is impacted by the post-glacial isostatic adjustment, with
269 present-day uplift in the Hudson Bay area of $\sim 10 \text{ mm year}^{-1}$ (e.g., Sella et al., 2007). Combining
270 satellite altimeter data with the Churchill tide-gauge data gives an uplift rate of about 9.0 ± 0.8
271 mm year^{-1} (Ray, 2015). The crustal uplift is evident in the negative sea level trend at Churchill of
272 about the same magnitude (Figure 3a). To examine synoptic to seasonal variability of sea level at

273 Churchill, a polynomial fit was subtracted from the data (Figure 3a). The polynomial fit better
 274 explains long-term variability of sea level at Churchill compared to the linear approximation,
 275 with respective coefficients of determination (R^2) of 0.41 and 39. Thus, in our study we
 276 examined the sea level anomalies (SLA) against the low-frequency trend conditioned by the
 277 post-glacial isostatic adjustment. In addition, the inverse barometer contribution to the water
 278 level record was removed ~~daily mean tide gauge data were corrected for inverted barometer~~
 279 ~~effect~~ using sea-level atmospheric pressure from the NCEP reanalysis. The mean correction
 280 attributed to inverted barometer effect was -1.19 ± 8.72 cm.

281 We used multiple linear regression to estimate a partial contribution of the cyclonic wind forcing
 282 and Churchill River discharge to SLA. In this context, multiple regression uses the least squares
 283 method to calculate the value of SLA based on the two independent variables as the vorticity
 284 index and Churchill River discharge.

285

286 4. Results

287 In this section, we examine the impact of ~~eyelonic~~ wind forcing and local river discharge on sea
 288 level variability at Churchill. We analyze (4.1) SLA at Churchill, (4.2) atmospheric vorticity
 289 over Hudson Bay, (4.3) the Churchill River discharge, and (4.4) their correlations.

290 4.1. Sea level

291 The 30-day running mean of SLA at Churchill ranging from 0.39 m in October 1973 to -0.36 m
 292 in April 1981 is dominated by the seasonal cycle (Figure 4a, blue line). In terms of the long-term
 293 monthly mean, sea level shows a seasonal cycle with positive anomalies > 0.09 m from
 294 September-November and negative anomalies of about -0.14 m from March-April (Figure 5a).

295 There is a substantial difference in the seasonal patterns of sea level between the pre- and post-
 296 diversion periods. The long-term variability of sea level (Figure 3a) and SLA (Figure 4a) shows
 297 no abrupt disruption with the introduction of the Churchill River diversion in 1977. However, the
 298 seasonal cycle of SLA generated for pre- and post-diversion shows a characteristic difference in
 299 the timing and magnitude of SLA (Figure 5a). First, for the natural seasonal cycle prior to 1977
 300 (blue line in Figure 5a), SLA shows two seasonal peaks in June (~ 0.04 m; standard error of the
 301 mean $\sigma = \pm 0.01$ cm) and November (~ 0.11 m, $\sigma = \pm 0.02$ cm). Post-diversion, SLA shows no
 302 peak in June, but the magnitude of positive anomalies in September and October increased to $>$
 303 0.08 m. This result is consistent with findings by *Gough and Robinson* (2000). In contrast to
 304 summer, during February-May, the pre- and post-diversion magnitude of SLA decreased and
 305 increased, respectively, by $\geq \pm 0.02$ m relative to the long-term monthly mean (Figure 5a). The
 306 standard deviation of the monthly mean values is up to 0.1 m (error bars in Figure 5a). The
 307 seasonal pattern of SLA was partially disrupted in 1981-82 and 1987-88, and significantly
 308 diminished in 1962-63 and 2016-17 (Figures 3a and 4a).

309 A closer look at the daily data reveals that the sea level seasonal maximum from October-
 310 November is modulated by storm surges frequently observed during the late fall. For example, in
 311 1969-70 and 2003-04 (highlighted with yellow shading on Figure 4), the seasonal cycle of sea

312 level (Figure 6, thick light blue line) was impacted by synoptic-scale events dominant during
 313 October-November (Figure 6, blue line). These storm surges lasted from ~3 to 6 days and
 314 correspond to positive anomalies of up to 0.5 m in the daily mean sea level (Figure 6b). In
 315 contrast, from December to May, the number and magnitude of storm surges gradually decrease
 316 (Figure 6).

317 4.2. Wind forcing

318 The vorticity index shows predominant cyclonic atmospheric circulation over Hudson Bay
 319 (mostly positive values in Figure 3a, red line), which agrees with results presented by *Saucier et*
 320 *al.* (2004) and *St-Laurent et al.* (2011). The strongest positive (cyclonic) vorticity is observed
 321 from fall 1962 to winter 1963 (vorticity index exceeded 14 s^{-1}), while the strongest negative
 322 (anticyclonic) atmospheric forcing (vorticity $< 4 \text{ s}^{-1}$) is recorded during summer 1963 (Figure
 323 3a). Overall, the alternation between monthly mean cyclonic and anticyclonic wind forcing is
 324 mostly governed by the seasonal cycle in vorticity (Figure 5b). The monthly mean **eyelonic**
 325 vorticity increases from 4 s^{-1} in September to $\sim 8 \text{ s}^{-1}$ in November, and then gradually returns to
 326 $\sim 4 \text{ s}^{-1}$ in February (Figure 5b). During March-May and August, **eyelonic**-vorticity is relatively
 327 low ($< 2 \text{ s}^{-1}$), and only in June and July does vorticity change to weak anticyclonic (slightly
 328 negative) values (Figure 5b). The seasonal cycle in atmospheric vorticity shows an insignificant
 329 difference pre- and post-diversion. From May to August and in December, there is no difference
 330 between the long-term monthly mean and monthly mean estimates for pre- and post-diversion
 331 (Figure 5b). For other months, the difference does not exceed $\pm 0.7 \text{ s}^{-1}$.

332 The interannual variability of wind forcing is mainly attributed to year-to-year changes in the
 333 cyclonic atmospheric circulation during fall-winter months. The seasonal amplitude of vorticity
 334 is significantly diminished in 1953-54, 2001-02 and 2015-2016 when the seasonal mean vorticity
 335 index for late fall to the beginning of winter did not exceed 8 s^{-1} (**black triangles in** Figure 3a). In
 336 contrast, during 1960-65, the vorticity seasonal cycle is amplified with the seasonal mean
 337 vorticity index between late fall and early winter up to 28 s^{-1} (**green triangles in** Figure 3a). The
 338 standard deviation of the monthly mean vorticity shown by error bars in Figure 5b gradually
 339 decreases from $\pm 4.5 \text{ s}^{-1}$ in December to $\pm 2.8 \text{ s}^{-1}$ in March-April.

340 Analysis of the daily vorticity time series sheds light on the origin of seasonality in vorticity.
 341 Positive seasonal anomalies from September-December (Figures 3a and 5b) are partly attributed
 342 to the occurrence of numerous vorticity peaks. For example, in 1969-70 and 2003-04
 343 (highlighted with yellow shading in Figure 3), the seasonal enhancement of atmospheric vorticity
 344 (Figure 6, thick pink line) was partially conditioned by synoptic-scale events recorded during
 345 October-November 1969 and 2003 (Figure 6, red line). The strongest vorticity peaks were
 346 observed on 18 October and 25 November 1969 ($> 4 \text{ s}^{-1}$; Figure 6a) and 15 October and 21
 347 November 2003 ($> 5 \text{ s}^{-1}$; Figure 6b). The SLP spatial distribution reveals that each of these peaks
 348 is attributable to a cyclone passing over Hudson Bay, with the center of low SLP located over the
 349 central Hudson Bay on 18 October and 25 November 1969 (Figures 7a and 7b, respectively) and
 350 15 October and 21 November 2003 (Figures 7c and 7d, respectively). The horizontal gradients of
 351 SLP over western Hudson Bay ranged from $0.020 \text{ hPa km}^{-1}$ (25 November 1969; Figure 7b) to
 352 $0.035 \text{ hPa km}^{-1}$ (21 November 2003; Figure 7d). Overall, from 1 September to 31 December,

353 vorticity exceeded 2 s^{-1} nine and 12 times in 1969 and 2003, respectively. In contrast, from 1
354 January to 30 April 1970 and 2004, vorticity exceeded 2 s^{-1} only four and seven times,
355 respectively (Figure 6). This suggests that the seasonal cycle in atmospheric vorticity is partially
356 governed by the number and strength of cyclones passing over Hudson Bay.

357 4.3. Local river discharge

358 The time series of Churchill River discharge (Figure 4a) is dominated by (i) the introduction of
359 the flow diversion in 1977 and (ii) the seasonal hydrologic cycle. The mean discharge dropped
360 by about one-third from $1,190 \text{ m}^3 \text{ s}^{-1}$ (1960-1976) to about $400 \text{ m}^3 \text{ s}^{-1}$ following the diversion in
361 1977. At the same time, the standard deviation of the mean discharge increased from about ± 300
362 to $\pm 470 \text{ m}^3 \text{ s}^{-1}$ following the diversion (Figure 4a). This is in line with results by *Déry et al.*
363 (2016). The mean annual timing of maximum river discharge during late spring to summer is not
364 significantly disrupted by the diversion (Figure 5c). The magnitude of the monthly mean
365 discharge pre- to post-diversion, however, reduces from about five-fold in March to about two-
366 and-a-half-fold in May-August (Figure 5c). After diversion, the standard deviation of the
367 monthly mean discharge doubles from May to October (Figure 5c). In contrast, from December
368 to April, the standard deviation of the monthly mean was not significantly impacted by the
369 diversion (Figure 5c).

370 4.4. Sea level response to wind forcing and local river discharge

371 Our data shows that SLA in Churchill, atmospheric vorticity over Hudson Bay, and Churchill
372 River discharge all show variability dominated by the seasonal cycle (Figures 3a, 4a, and 5). In
373 what follows, SLA at Churchill is first compared to the atmospheric vorticity, and then to the
374 Churchill River discharge, with a main focus on the seasonal cycle.

375 The correlation between the daily vorticity index and SLA from 1950-2019 and 1960-2019 is
376 0.48 and 0.47, respectively, with insignificant differences between correlations estimated for
377 periods pre- and post-diversion (0.49 and 0.47, respectively; Figure 3b and Table 1). For the ice-
378 free period from June to November, correlations for whole period, and pre- and post-diversion
379 increase to 0.54, 0.52 and 0.55 (Table 2), respectively, compared to 0.47, 0.49 and 0.47 for the
380 ice-covered period from December to May (Table 3). We test the difference between correlations
381 estimated for the ice-covered and ice-free seasons using the Fisher z-transformation (*Fisher,*
382 1921). Statistical assessment shows that the only differences between correlations estimated for
383 whole period and post-diversion are statistically significant at the 99% confidence level.

384 The relationship between vorticity and SLA changes significantly from one year to another. The
385 mean annual correlations in Figure 3b show these differences ranging from 0.18 in 1982 to 0.69
386 in 1991. During periods when the sea level seasonal cycle almost disappears (1981-82 and 1987-
387 88), the mean annual correlation drops to about 0.3 and 0.4, respectively (Figure 3b). When the
388 sea level seasonal cycle is diminished (1962-63 and 2016-17), a modest correlation of ~ 0.5 is
389 estimated (Figure 3b). For time periods enlarged in Figure 6, the annual mean correlation
390 significantly exceeds the long-term mean of 0.47, attaining 0.65 and 0.57 for 1969-70 and 2004-
391 05, respectively (Figure 3b). The direct linkage between vorticity and SLA is evident in Figure 6.
392 During September-November 1969 and 2003, all significant synoptic peaks in SLA are

393 consistent with those in atmospheric vorticity, including storm surges on 18 October and 25
394 November 1969 (Figure 6a) and on 15 October and 21 November 2003 (Figure 6b).

395 In contrast to atmospheric vorticity, the correlation between daily SLA and river discharge is
396 significantly smaller. Through the full record from 1960 to 2019, the correlation is 0.22, with an
397 insignificant difference between pre- and post-diversion (0.20 and 0.23, respectively, Figure 4b
398 and Table 1). For the ice-free period from June to November, correlations drop close to or below
399 the level of statistically significant values for the whole and pre-diversion periods (0.08 and 0.03,
400 respectively), and to 0.11 post-diversion (Table 2) compared to 0.21, 0.12 and 0.19 for the ice-
401 covered period from December to May (Table 3). Note that the difference between correlations
402 estimated for the ice-covered and ice-free seasons is statistically significant for only 1960-2019.

403 Similar to the linkage between vorticity and SLA, the relationship between river discharge and
404 SLA shows significant interannual variability. Correlations computed through the 365-day
405 moving window show negative to positive values ranging from -0.3 to 0.7 with about 15% of
406 estimates below the level of statistical significance (Figure 4b). Among all events when the
407 amplitude of the sea level seasonal cycle was strongly reduced, only 1962-63 and 1981-82 show
408 statistically significant correlation between river discharge and SLA of ~ 0.25 (Figure 4b). For
409 events in 1987-88 and 2016-17, correlation is relatively close to or below the level of statistical
410 significance (Figure 4b). The interannual difference in contribution of river discharge to the sea
411 level variability is also evident for 1969-70 and 2004-05. In 1969-70, the annual mean
412 correlation shows relatively modest contributions of river discharge to sea level variability
413 (correlation $R \sim 0.29$; Figure 4b) as compared to correlation with atmospheric vorticity ($R \sim 0.65$;
414 Figure 3b). In 2004-05, however, there is no correlation between SLA and river discharge
415 (Figure 4b), and sea level variability is impacted by wind forcing ($R = 0.57$; Figure 3b).

416 Overall, our results show that the wind forcing impacts the synoptic and seasonal variability of
417 sea level. In what follows, we use the coefficient of determination (R^2 , where R is correlation
418 coefficient in Tables 1-3) to describe the proportion of the variance in sea level that is explained
419 by the wind forcing, river discharge, and the wind forcing and river discharge together. Through
420 the whole annual cycle from 1960 to 2019, wind forcing explains about 22% of sea level
421 variability, while river discharge contributes only $\sim 5\%$. Multiple regression analysis shows that
422 on average, both explain $\sim 28\%$ of sea level variability (Table 1).

423 Our results also reveal the important role of sea-ice cover and river diversion in modifying
424 controls on sea level variability. During the ice-free seasons from 1960-1976, the contribution of
425 wind forcing is 27%, and the role of river discharge is negligible (Table 2). Post-diversion,
426 cyclonic wind forcing and river discharge contribute 30% and 1%, respectively. Together they
427 explain up to 32% of sea level variability (Table 2). During the ice-covered season, the
428 contribution of vorticity is reduced to 22%, with insignificant difference between pre- and post-
429 diversion (Table 3). The contribution of river discharge varies from 1% for pre-diversion to 4%
430 for post-diversion. Wind and river forcing together explain $\sim 27\%$ of sea level variability for both
431 pre- and post-diversion periods (Table 3). Summarizing these results, we point out that the sea-
432 ice cover reduces the influence of wind forcing, and the influence of local river discharge is
433 slightly increased primarily during the ice covered post-diversion period. Post-diversion, the

434 magnitude of river discharge was reduced about three-fold, but seasonal variability increased by
435 a factor of 1.5 (Figure 4a and *Déry et al.*, 2016). Thus, we attribute the increase in river
436 discharge forcing during the post-diversion period mainly to the higher variability in river
437 discharge from May to November (Figure 4a, 5c, and *Déry et al.*, 2016). Note that during May
438 about 85% of Hudson Bay is ice covered (*Tivy et al.*, 2010), and the standard deviation of the
439 monthly mean discharge in May increases from about ± 170 pre-diversion to ± 380 $\text{m}^3 \text{s}^{-1}$ post-
440 diversion.

441

442 5. Discussion

443 Our results show that sea level variability at Churchill is ~~rather influenced primarily impacted~~ by
444 wind forcing, with discharge from the Churchill River playing a secondary role. Overall, the
445 atmospheric vorticity explains up to 30% of sea level variability at Churchill, with local river
446 discharge contributing up to only 5% (Tables 1-3). This suggests that in western Hudson Bay the
447 northerly winds associated with cyclonic wind forcing (Figure 2b) generate storm surge along
448 the coast due to a surface Ekman on-shore transport. This is consistent with results from
449 *Dmitrenko et al.* (2020), who used mooring records and Churchill tide gauge observations in
450 2016-17 to identify this mechanism. A direct response of the water level to balance wind stress
451 acting on the surface does not play a role for generating SLA because there is no correlation
452 between SLA and zonal wind (not shown).

453 The SLA seasonal cycle in Figure 5a is only partially explained by seasonality in ~~eyclonic~~ wind
454 forcing and local river discharge. The SLA seasonal cycle is also consistent with summertime
455 warming and freshening, and wintertime cooling and salinification. During the ice-free summer
456 period, the water column warms, and seawater becomes less dense and expands, causing the
457 thermosteric sea-level rise. In addition, during summer, riverine water and sea-ice meltwater
458 decrease salinity of the Bay, thus, causing the halosteric sea-level rise. It seems that these factors
459 can explain the ~~significant residual~~ fraction of the SLA seasonal variability that is not explained
460 by wind forcing and local river discharge. However, the detailed assessment of the thermosteric
461 and halosteric contributions to the Hudson Bay sea level variability is beyond the scope of this
462 paper. In this context, we point out that we examine only the direct impact of the river discharge
463 on the sea level in the Churchill River mouth ignoring the cumulative effect of riverine water on
464 steric height. This simplification seems to be reasonable because the residence time of the
465 riverine water fraction in southwestern Hudson Bay during summer is ~ 1 -3 months (*Granskog et*
466 *al.*, 2009).

467 For the seasonal time scales, increased cyclonic activity during fall to early winter impacts the
468 seasonal cycle in SLA. In contrast to *Gough and Robinson* (2000), we assert that a positive SLA
469 from September-November (Figure 5a) is attributed to enhanced atmospheric vorticity rather
470 than to the local river discharge. The signature of the local river discharge is, however, traceable
471 through the SLA seasonal cycle. During the pre-diversion period, positive SLA in June (Figure
472 5a) appears to be linked to the spring freshet of the Churchill River (Figures 5a and 5c).
473 However, post-diversion this positive SLA in June vanishes due to the abrupt decrease in the

474 Churchill River discharge during the spring freshet from $\sim 1,500$ to $700 \text{ m}^3 \text{ s}^{-1}$ (Figure 5c).
475 Gradual decreases in Churchill River discharge from June/July to April for both pre- and post-
476 diversion cannot explain the positive SLA from fall to winter, especially during the post-
477 diversion period when the mean annual Churchill River discharge decreases to $\sim 400 \text{ m}^3 \text{ s}^{-1}$
478 (Figure 5c). Note that the cumulative effect of riverine water on steric height is neglected.

479 An additional perspective on SLA response to atmospheric and river forcing comes from a
480 comparison of the monthly mean vorticity and Churchill River discharge time series' with SLA
481 at Churchill for the whole period of river discharge observations, and the pre- and post-diversion
482 periods (Figures 8a, 8b, and 8c, respectively). The SLA patterns for the whole period of river
483 discharge observation (Figure 8a) are strongly impacted by changes in the magnitude of
484 discharge during the pre- and post-diversion periods, as previously discussed. In contrast, the
485 SLA patterns compiled for the pre- and post-diversion periods (Figures 8b and 8c, respectively)
486 provide more precise features of the SLA response to atmospheric and river forcing. In general,
487 comparing atmospheric vorticity to sea level at Churchill shows that cyclones generate positive
488 SLA up to 0.15 m (Figure 8c). The maximum SLA response to cyclonic atmospheric forcing is
489 observed during the ice-free period (pink shading and white circles in Figures 8b and 8c), which
490 is consistent with results of the correlation analysis (Tables 2 and 3). The combination of
491 anticyclonic (negative) vorticity and low river discharge generates negative SLA up to 0.09 m
492 during both ice-free and ice-covered seasons (blue shading in Figures 8b and 8c).

493 The zero SLA contour in Figure 8b and 8c is displaced relative to the zero vorticity and the long-
494 term mean river discharge for the pre- and post-diversion periods. This indicates that these two
495 predictors alone are insufficient to entirely explain the sea level variability, and that there must
496 be other contributing factors. Correlation analysis (Tables 2 and 3) suggests that sea-ice also
497 plays a role in modifying the impact of atmospheric forcing on SLA. In this context, Figures 8
498 reveals the role of sea-ice cover for generating the SLA. The sea level at Churchill exhibits
499 negative SLA while atmospheric vorticity is positive, but not exceeding $\sim 6\text{-}8 \text{ s}^{-1}$ (Figure 8). This
500 situation is usually observed during the ice-covered season when river discharge is below the
501 annual mean (blue circles and blue shading in Figures 8b and 8c). We attribute this disruption to
502 the sea-ice cover. Throughout the entire year, positive SLA is generated in response to strong
503 cyclones with vorticity exceeding $\sim 6\text{-}8 \text{ s}^{-1}$ regardless of the river discharge contribution and sea-
504 ice conditions (red shading in Figure 8 for vorticity $> \sim 6\text{-}8 \text{ s}^{-1}$). During the ice-covered season, at
505 relatively low river discharge ($< 1,200 \text{ m}^3 \text{ s}^{-1}$ and $350 \text{ m}^3 \text{ s}^{-1}$ for pre- and post-diversion,
506 respectively), negative SLA is associated with positive vorticity $< 6\text{-}8 \text{ s}^{-1}$ (blue circles and blue
507 shading in Figures 8b and 8c). Thus, vorticity $\sim 6\text{-}8 \text{ s}^{-1}$ is suggested to be a very rough estimate of
508 the vorticity threshold attributed to the sea-ice impact. Above this threshold, sea-ice does not
509 eliminate wind stress from the water column, and wind forcing impacts sea level variability in
510 Churchill year-round. Below this threshold, sea-ice eliminates wind forcing and a negative SLA
511 is conditioned by low river discharge. In fact, extension of the landfast ice as well as sea-ice
512 roughness and concentration can play a role modifying the thresholds at which wind impacts the
513 SLA. When the Churchill River discharge exceeds the monthly means of $1,500\text{-}1,600 \text{ m}^3 \text{ s}^{-1}$ and
514 $\sim 900 \text{ m}^3 \text{ s}^{-1}$ for pre- and post-diversion periods, respectively, positive SLA results regardless of
515 wind forcing.

516 Our results on the mechanisms of sea level variability at Churchill differ from those obtained by
517 *Gough and Robinson* (2000). First, using sea level and river discharge data from 1974-1994, they
518 found that correlation between Churchill River discharge and SLA in Churchill explains 43% of
519 sea level variability (versus the 5% derived in our analysis). Second, *Gough and Robinson*
520 (2000) explain a positive SLA observed in Churchill from October-November by the river
521 discharge pulse into the James Bay region with an advective lag of ~4-5 months. Furthermore,
522 *Gough et al.* (2005) speculate that positive SLA during fall is attributed to the James Bay
523 riverine water fraction, which does not exit the Bay through Hudson Strait, but instead re-
524 circulates in western Hudson Bay. The halosteric sea level changes associated with this
525 freshwater fraction are suggested to generate a positive SLA observed in Churchill from
526 October-November. The pathway of this water and the reason for disrupting the mean cyclonic
527 circulation in the Bay were, however, neither specified in *Gough and Robinson* (2000) nor in
528 *Gough et al.* (2005). The distance from James Bay to Churchill measured along the coast is
529 roughly 1,000 km. For a 120-150-day lag between peaks in river discharge to James Bay in June
530 (*Déry et al.*, 2005) and maximum positive SLA at Churchill in November, this distance suggests
531 the unrealistic rate of mean advective velocity to be ~8-10 cm s⁻¹. Note that *Dmitrenko et al.*
532 (2020) estimated the velocity of the northward flow along the western coast of Hudson Bay
533 during strong cyclonic storms to ~13 cm s⁻¹, which significantly exceeds the annual mean
534 meridional transport of ~1-2 cm s⁻¹.

535 Overall, the hypothesis by *Gough and Robinson* (2000) and *Gough et al.* (2005) about the
536 linkage between the river discharge pulse into James Bay and a positive SLA in Churchill is
537 suggestive of the seasonal disruption of the Hudson Bay cyclonic circulation that is in line with
538 the seasonal pattern of atmospheric vorticity in Figure 5b. Based on satellite altimetry and
539 numerical simulation, *Ridenour et al.* (2019a) revealed a seasonal reversal to anticyclonic
540 circulation in southwestern Hudson Bay from May-July, with a return to strong cyclonic
541 circulation in fall in response to the seasonal patterns of surface stress. This is consistent with the
542 seasonal cycles of vorticity presented in Figure 5b. However, among ~120-150 days of the
543 hypothetical transit time from James Bay to Churchill, the anticyclonic atmospheric forcing is
544 persistently observed only during May-July; in August, vorticity returns to cyclonic (Figure 5b).
545 In the three months before the occurrence of the positive SLA at Churchill in November, the
546 atmospheric forcing has already returned to cyclonic (Figure 5b). In this context, the hypothesis
547 by *Gough and Robinson* (2000) and *Gough et al.* (2005) linking SLA in Churchill to river
548 discharge in James Bay seems to be inconsistent. In what follows, we provide additional
549 arguments to support our finding on the role of wind forcing in generating the SLA at Churchill.

550 First, *Tushingham* (1992) provide the time series of sea level at Churchill and the Churchill River
551 discharge from 1972 to 1989 (Figure 5 from *Tushingham*, 1992). These time series' clearly show
552 an overall low positive correlation completely disrupted in 1973-74, 1977, and 1987-86, which is
553 consistent with our analysis (Figure 4). For 1973-74 and 1987-86, the annual-mean correlation
554 was estimated to be about -0.1 and is below the level of statistical significance (Figure 4b).
555 Overall, from 1960 to 2019, there were 19 events that lasted up to 1.8 years in duration when
556 correlations between the SLA and river discharge were statistically insignificant or even negative
557 (Figure 4b). This calls into question the correlations between Churchill River discharge and SLA

558 in Churchill reported by Gough and Robinson (2000) and Gough et al. (2005). Note that the
559 period from 1972 to 1989 used by *Tushingham* (1992) overlaps with the majority of the period
560 from 1974 to 1994 used by *Gough and Robinson* (2000).

561 Second, *Ward et al.* (2018) analyzed daily data from the Global Runoff Data Centre for 187
562 stations including Churchill and daily maxima sea level data from the Global Extreme Sea-level
563 Analysis. They found no statistically significant dependence between annual maxima of the
564 Churchill River discharge and sea level. For comparison, along the Pacific coast of North
565 America, the correlation ranged from 0.2 to 0.4, and accounted for 4-16% of the variation in sea
566 level. This is consistent with a previous concern about significant impact of Churchill River
567 discharge on SLA in Churchill.

568 Third, our analysis shows that the seasonal cycle in sea level variability with positive SLA
569 during fall is observed not only in Churchill, but also along the eastern coast of Hudson Bay in
570 Innujuak (Figures 1 and 9). While the sea level record at Innujuak is short and not continuous,
571 a positive SLA is recognizable during fall 1969-70 and 1973-76 (Figure 9, blue line). Note that
572 the seasonal SLA at Innujuak cannot be generated locally because the annual mean (1964-2000)
573 discharge of the local Innujuak River is only $3.3 \text{ km}^3 \text{ year}^{-1}$, about three times smaller than the
574 Churchill River discharge post-diversion (*Godin et al.*, 2017). In contrast, the seasonal pattern in
575 SLA at Innujuak is generated by the same cyclonic forcing as in Churchill. Seasonal SLA in
576 Innujuak is consistent with seasonal amplification of atmospheric vorticity (Figures 5b and 9).
577 Moreover, in Innujuak, the sea level peaks on 18 October and 25 November 1969 are coherent
578 with peaks in atmospheric vorticity (Figure 9) and sea level at Churchill (Figure 6a). From the
579 preceding analysis we explicitly know that these two vorticity peaks were generated by cyclones
580 passing over the Bay (Figure 7a). The coherent peaks in sea level in Churchill and Innujuak
581 suggest that cyclones that were centered over Hudson Bay on 18 October and 25 November 1969
582 generated storm surge on both the eastern and western coasts of Hudson Bay. This is also
583 supported by a coherent response of sea level to atmospheric forcing at Cape Jones Island and
584 North Kopak Island (Figures 1 and 9). Our hypothesis is also consistent with results of sea level
585 numerical simulations in response to cyclones passing over the Bay in 2016-17 (*Dmitrenko et al.*,
586 2020). For synoptic storm surges, on-shore Ekman transport increases the mass of water column
587 along the coast (the barotropic component). The seasonal baroclinic component appears during
588 summer when water is fresher and warmer causing the thermosteric and halosteric sea-level rise
589 along the coast.

590 Fourth, satellite altimetry reveals a spatially uniform response of sea level to the seasonal cycle
591 in atmospheric vorticity along the whole coast of Hudson Bay (Figure 10). For 1993-2020, we
592 examine the difference between the sea surface heights (SSH) during summer, when monthly
593 mean atmospheric vorticity changes from -0.7 s^{-1} in June to 1.1 s^{-1} in August, and fall, when
594 vorticity increases from 4.2 s^{-1} in September to 7.3 s^{-1} in November (Figure 5b). Results suggest
595 that enhanced cyclonic vorticity during fall generates seasonal SSH elevation over the entire
596 coast of Hudson Bay with SSH differences between fall and summer ranging from $>5 \text{ cm}$ in
597 James Bay to $\sim 1 \text{ cm}$ along the northwest coast (Figure 10). This confirms our results that a
598 positive SLA during fall is generated over the entire coast of Hudson Bay, and particularly in

599 Churchill and Innukjuak, in response to enhanced cyclonic wind forcing (Figures 5a, 5b, and 9).
600 Overall, our third and fourth points suggest that the hypothesis of Gough and Robinson (2000)
601 and Gough et al. (2005) about a linkage between river discharge into James Bay and SLA in
602 Churchill is inconsistent.

603 One may suggest that seasonal SSH elevation in Figure 10 can be partly due to the thermosteric
604 and halosteric sea-level rise. During summer, the Hudson Bay coastal domain receives large
605 amount of fresh and warm water from river runoff. The seasonal tendency for river discharge,
606 however, is opposite to that for the SSH in Figure 10. For 1988-2000, Déry et al. (2005) reported
607 that the total discharge of rivers flowing into Hudson Bay peaks in June at $\sim 3.6 \text{ km}^3 \text{ day}^{-1}$, which
608 significantly exceeds the secondary maximum in October ($\sim 2.3 \text{ km}^3 \text{ day}^{-1}$). The seasonal mean
609 total river discharge in September-November ($\sim 1.9 \text{ km}^3 \text{ day}^{-1}$) is one-and-a-half times smaller
610 compared to $\sim 2.8 \text{ km}^3 \text{ day}^{-1}$ in June-August. Based on these estimates, the river discharge
611 seasonal cycle in June-November is inconsistent with that for the SSH in Figure 10. The
612 cumulative effect of river discharge on the seasonal cycle can play a role, but the residence time
613 of the riverine water fraction in southwestern Hudson Bay during summer is relatively small (~ 1 -
614 3 months; Granskog et al., 2009).

615 Finally, our results on the atmospheric forcing of the Hudson Bay SLA are in agreement with
616 conclusions by Piecuch and Ponte (2014, 2015). Using ocean mass measurements from satellite
617 gravimetry conducted during the Gravity Recovery and Climate Experiment, they found that
618 wind forcing dominates sea-level and mass variability in Hudson Bay, and wind might drive
619 Hudson Bay mass changes due to wind-driven outflow through Hudson Strait (Piecuch and
620 Ponte; 2014). For the sea level interannual variability in Hudson Bay, also evident in Figure 4a,
621 Piecuch and Ponte (2015) revealed a wind-driven barotropic fluctuation that explains most of the
622 non-seasonal sea level variance. Furthermore, they suggest that anomalous inflow and outflow
623 through Hudson Strait, which impacts sea level variability in Hudson Bay, are driven by wind
624 stress over Hudson Strait. This highlights the role of wind forcing in amplifying the freshwater
625 outflow from Hudson Bay, as also suggested by Straneo and Saucier (2008) and Dmitrenko et al.
626 (2020).

627 In summary, we suggest that seasonal amplification of atmospheric vorticity, partially
628 conditioned by the number and strength of cyclones passing over the Bay during fall to early
629 winter, generates the seasonal cycle in sea level variability over the entire Bay as depicted
630 schematically in Figure 11. Cyclones passing over Hudson Bay during fall to early winter cause
631 on-shore Ekman transport and storm surges over the entire coast of Hudson Bay (Figure 11a). In
632 summer, anticyclonic wind forces off-shore Ekman transport lowering sea level along the coastline
633 of Hudson Bay (Figure 11b).

634

635 **Summary and conclusions**

636 Our analysis revealed that in contrast to previous research, the local Churchill River discharge
637 explains only up to 5% of the sea level variability at Churchill. ~~While, e~~Cyclonic atmospheric
638 forcing is shown to explain from 22% during the ice-covered winter-spring season to 30% during

639 the ice-free summer-fall season (Tables 1-3). Multiple regression analysis showed that
640 atmospheric forcing and local river discharge together can explain up to 32% of the sea level
641 variability at Churchill. We found that a positive sea level anomaly in Churchill during fall is
642 partially conditioned by the seasonal cycle in atmospheric vorticity, with prevailing cyclonic
643 wind forcing during fall to the beginning of winter (Figure 5). Sea-ice cover reduces wind stress
644 on the water column during the ice-covered season from December to May, and cyclonic wind
645 forcing generates positive sea level anomalies at Churchill when only the monthly mean vorticity
646 exceeds $\sim 6\text{-}8\text{ s}^{-1}$ (Figure 8). In this context, transition towards a longer open water season (e.g.,
647 Hochheim and Barber, 2014) is expected to increase the contribution of atmospheric forcing to
648 sea level variability.

649 We expanded our observations at Churchill to the bay-wide scale using sea level observations
650 along the eastern coast of the Bay and satellite altimetry. A coherent sea level response to
651 atmospheric forcing observed at the opposite sides of Hudson Bay suggests that the spatial scale
652 of cyclones passing over Hudson Bay roughly equals the Hudson Bay area (Figures 7 and 9, and
653 *Dmitrenko et al.*, 2020). This scaling equivalency implies that cyclones passing over Hudson Bay
654 cause on-shore Ekman transport and storm surges over the entire Hudson Bay coast (Figure 11a).
655 This is also consistent with results by *Dmitrenko et al.* (2020) obtained for 2016-17. Moreover,
656 the satellite altimetry data shows that this scaling equivalency works not only for synoptic, but
657 also for the seasonal time scale. The seasonal cycle in atmospheric vorticity (Figure 5b) partially
658 conditions the seasonal cycle in sea level variability over the entire coast of Hudson Bay. The
659 recurring cyclonic wind forcing during fall favors sea level elevation over the entire Hudson Bay
660 coast compared to summer (Figures 10 and 11). This seasonal pattern in sea-level variability
661 seems to have ~~has an important~~ implication for geostrophic circulation. The cross-shelf pressure
662 gradient generated due to seasonal amplification of sea level along the coast drives alongshore
663 geostrophic flow and favors the cyclonic circulation around Hudson Bay during fall to earlier
664 winter. In contrast, during summer the geostrophic component attributed to the anticyclonic
665 atmospheric forcing disrupts the Hudson Bay cyclonic circulation as shown by *Ridenour et al.*
666 (2019a).

667 Our research is important for maritime activity within the Bay. Communities around the Bay
668 highly rely on the annual summer sea-lift to re-supply them at a fraction of the price compared to
669 air transport (*Kuzyk and Candlish*, 2019). In this context, positive coastal sea level anomalies
670 during fall favor re-supply operations to coastal communities. However, increased cyclonic
671 activity during fall is also associated with extreme wind events (Figure 2b) and storm surges
672 (e.g., Figure 6) increasing risks to re-supply and fuel-transfer operations.

673 The origin of seasonality in ~~eyelonie~~ wind forcing, its climatic aspects and ocean response to
674 seasonal and interannual variability in atmospheric vorticity over the Bay are among important
675 priorities for our future research. The freshwater storage in Hudson Bay and export through
676 Hudson Strait seem to be directly impacted by seasonal and interannual variability in wind
677 forcing, clearly defining the need for further research in this area using multi-year numerical
678 simulations and atmospheric reanalyses. Seasonality of the wind forcing is the hypothesized
679 cause of the sea level variability, but probably does not provide a complete explanation. The

680 steric changes in coastal zone attributed to river runoff were not taken into account that points
681 out a necessity for future research involving numerical simulations. Possible impacts of climate
682 change on cyclone activity in Hudson Bay, and therefore sea-level variability, will be addressed
683 in future research.

684

685 **Data availability**

686 Sea level data used in this study are available from the Canadian Tides and Water Levels Data
687 Archive of the Fisheries and Oceans Canada through [http://www.isdm-gdsi.gc.ca/isdm-gdsi/twl-](http://www.isdm-gdsi.gc.ca/isdm-gdsi/twl-mne/index-eng.htm#s5)
688 [mne/index-eng.htm#s5](http://www.isdm-gdsi.gc.ca/isdm-gdsi/twl-mne/index-eng.htm#s5) (last access: 26 August 2021). The daily SLA/ADT maps with all
689 corrections applied are distributed via CMEMS (<https://marine.copernicus.eu/>; last access: 26
690 August 2021). Churchill River discharge data are provided in supplementary material. SLP and
691 wind data are available from the <https://psl.noaa.gov/data/composites/hour/> and
692 <https://psl.noaa.gov/cgi-bin/data/testdap/timeseries.pl> (last access: 26 August 2021).

693

694 **Author contributions**

695 Conceptualization: ID; methodology: ID, DV, TS, AT; formal analysis: ID, DV, AT;
696 investigation: ID, DV, AC, TS; resources: KS, DBarber; data curation: ID, DV, AT; writing
697 (original draft): ID, DV, TS; writing (review & editing): AC, DV, SK, TS, AT, DBabb;
698 visualization: ID, DV; supervision: DBarber; project administration: KS, DBarber; funding
699 acquisition: KS, DBarber.

700

701 **Competing interests**

702 The authors declare that they have no conflict of interest.

703

704 **Acknowledgments**

705 This work is a part of research conducted under the framework of the Arctic Science Partnership
706 (ASP) and ArcticNet. This research is also a contribution to the Natural Sciences and
707 Engineering Council of Canada (NSERC) Collaborative Research and Development project:
708 BaySys (CRDPJ470028-14). Funding for this work was provided by NSERC, Manitoba Hydro,
709 the Canada Excellence Research Chair (CERC) program, the Canada Research Chairs (CRC)
710 program and the Canada-150 Research Chairs program. D. Babb is additionally supported by
711 NSERC and the Canadian Meteorological and Oceanographic Society (CMOS). DLV was
712 supported by NOAA Atlantic Oceanographic and Meteorological Laboratory under the auspices
713 of the Cooperative Institute for Marine and Atmospheric Studies (CIMAS), a cooperative
714 institute of the University of Miami and NOAA, cooperative agreement NA20OAR4320472.

715

716 **References**

717 Andrews, J., Babb, D., and Barber, D. G.: Climate change and sea ice: Shipping accessibility on
718 the marine transportation corridor through Hudson Bay and Hudson Strait (1980 –2014), *Elem.*
719 *Sci. Anth.*, 5, 15, <https://doi.org/10.1525/elementa.13>, 2017.

720 [CLS-DOS: Validation of altimeter data by comparison with tide gauge measurements: yearly](#)
721 [report 2016, Ref. CLS-DOS-17-0016, available at:](#)
722 [https://www.aviso.altimetry.fr/fileadmin/documents/calval/validation_report/annual_report_TG_](https://www.aviso.altimetry.fr/fileadmin/documents/calval/validation_report/annual_report_TG_2016.pdf)
723 [2016.pdf](https://www.aviso.altimetry.fr/fileadmin/documents/calval/validation_report/annual_report_TG_2016.pdf), 2016, last access: 26 August 2021.

724 Copernicus Climate Change Service (C3S): ERA5: Fifth generation of ECMWF atmospheric
725 reanalyses of the global climate. Copernicus Climate Change Service Climate Data Store (CDS),
726 2017, available at <https://cds.climate.copernicus.eu/cdsapp#!/home>, last access: 26 August 2021.

727 Déry, S. J., Stieglitz, M., McKenna, E. C., and Wood, E. F.: Characteristics and trends of river
728 discharge into Hudson, James, and Ungava Bays, 1964–2000, *J. Climate*, 18, 2540–2557,
729 <https://doi.org/10.1175/JCLI3440.1>, 2005.

730 Déry, S. J., Mlynowski, T. J., Hernández-Henríquez, M. A., and Straneo, F.: Interannual
731 Variability and Interdecadal Trends in Hudson Bay Streamflow, *Journal of Marine Systems*, 88
732 (3), 341–351, <https://doi.org/10.1016/j.jmarsys.2010.12.002>, 2011.

733 Déry, S. J., Stadnyk, T. A., MacDonald, M. K., and Gaudi-Sharma, B.: Recent trends and
734 variability in river discharge across northern Canada, *Hydrology and Earth System Sciences*, 20,
735 4801–4818, <https://doi.org/10.5194/hess-20-4801-2016>, 2016.

736 Dmitrenko, I. A., Kirillov, S. A., and Tremblay, L. B.: The long-term and interannual variability
737 of summer fresh water storage over the eastern Siberian shelf: Implication for climatic change, *J.*
738 *Geophys. Res.*, 113, C03007, <https://doi.org/10.1029/2007JC004304>, 2008a.

739 Dmitrenko, I. A., Kirillov, S. A., Tremblay, L. B., Bauch, D., and Makhotin, M.: Effects of
740 atmospheric vorticity on the seasonal hydrographic cycle over the eastern Siberian shelf,
741 *Geophys. Res. Lett.*, 35, L03619, <https://doi.org/10.1029/2007GL032739>, 2008b.

742 Dmitrenko, I. A., Myers, P. G., Kirillov, S. A., Babb, D. G., Volkov, D. L., Lukovich, J. V., Tao,
743 R., Ehn, J. K., Sydor, K., and Barber, D. G.: Atmospheric vorticity sets the basin-scale
744 circulation in Hudson Bay, *Elem. Sci. Anth.*, 8, 49, <https://doi.org/10.1525/elementa.049>, 2020.

745 Dmitrenko, I. A., Kirillov, S. A., Babb, D. G., Kuzyk, Z. A., Basu, A., Ehn, J. K., Sydor, K., and
746 Barber D. G.: Storm-driven hydrography of western Hudson Bay, ~~submitted to~~ *Continental Shelf*
747 *Res.*, [227, 104525, https://doi.org/10.1016/j.csr.2021.104525, 2021.](#)

748 Eastwood, R. A., McDonald, R., Ehn, J., Heath, J., Arragutainaq, L., Myers, P. G., Barber, D.,
749 and Kuzyk, Z. A.: Role of river runoff and sea-ice brine rejection in controlling stratification
750 throughout winter in southeast Hudson Bay, *Estuaries and Coasts*, 43, 756–786,
751 <https://doi.org/10.1007/s12237-020-00698-0>, 2020.

- 752 Fisher, R. A.: On the 'probable error' of a coefficient of correlation deduced from a small sample,
753 *Metron*, 1, 3–32, 1921.
- 754 Godin, P., Macdonald, R. W., Kuzyk, Z. Z. A., Goñi, M. A., and Stern, G. A.: Organic matter
755 compositions of rivers draining into Hudson Bay: Present-day trends and potential as recorders
756 of future climate change, *J. Geophys. Res. Biogeosci.*, 122, 1848–1869,
757 <https://doi.org/10.1002/2016JG003569>, 2017.
- 758 Gough, W. A.: Projections of sea-level change in Hudson and James Bays, Canada, due to global
759 warming, *Arctic and Alpine Research*, 30(1), 84–88, <https://doi.org/10.2307/1551748>, 1998.
- 760 Gough, W. A., and Robinson, C. A.: Sea-level Variation in Hudson Bay, Canada, from Tide-
761 Gauge Data, *Arctic, Antarctic, and Alpine Research*, 32(3), 331–335,
762 <https://doi.org/10.1080/15230430.2000.12003371>, 2000.
- 763 Gough, W. A., Robinson, C., and Hosseinian, R.: The Influence of James Bay River Discharge
764 on Churchill, Manitoba Sea Level, *Polar Geography*, 29(5), 213–223,
765 <https://doi.org/10.1080/789610202>, 2005.
- 766 Granskog, M. A., Macdonald, R. W., Kuzyk, Z. A., Senneville, S., Mundy, C.-J., Barber, D. G.,
767 Stern, G. A., and Saucier, F.: Coastal conduit in southwestern Hudson Bay (Canada) in summer:
768 Rapid transit of freshwater and significant loss of colored dissolved organic matter, *J. Geophys.*
769 *Res.*, 114, C08012, <https://doi.org/10.1029/2009JC005270>, 2009.
- 770 Granskog, M. A., Kuzyk, Z. A., Azetsu-Scott, K., and Macdonald, R. W.: Distributions of
771 runoff, sea-ice melt and brine using $\delta^{18}\text{O}$ and salinity data - A new view on freshwater cycling
772 in Hudson Bay, *Journal of Marine Systems*, 88, 362–374,
773 <https://doi.org/10.1016/j.jmarsys.2011.03.011>, 2011.
- 774 Guttenberg, B.: Changes in sea level, postglacial uplift, and mobility of the earth's interior,
775 *Geological Society of America Bulletin*, 52(5), 721–772, <https://doi.org/10.1130/GSAB-52-721>,
776 1941.
- 777 Hersbach, H., and Coauthors: The ERA5 global reanalysis, *Quarterly Journal of the Royal*
778 *Meteorological Society*, 146, 1999–2049, <https://doi.org/10.1002/qj.3803>, 2020.
- 779 Hochheim, K. P., and Barber, D. G.: Atmospheric forcing of sea ice in Hudson Bay during the
780 fall period, 1980–2005. *J. Geophys. Res.*, 115, C05009, <https://doi.org/10.1029/2009JC005334>,
781 2010.
- 782 Hochheim, K. P., and Barber, D. G.: An update on the ice climatology of the Hudson Bay
783 System. *Arctic Antarctic Alpine Res.*, 46(1), 66–83, <https://doi.org/10.1657/1938-4246-46.1.66>,
784 2014.
- 785 Ingram, R. G. and Prinsenberg, S.: Coastal oceanography of Hudson Bay and surrounding
786 Eastern Canadian Arctic Waters, In: Robinson, A. R. and K. N. Brink (Eds.), *The Sea*, Vol. 11.
787 *The Global Coastal Ocean Regional Studies and Synthesis*. Harvard University Press,
788 Cambridge, Massachusetts and London, 835–861, 1998.

- 789 Joyce, B. R., Pringle, W. J., Wirasaet, D., Westerink, J. J., Van der Westhuysen, A. J., Grumbine,
790 R., and Feyen, J.: High resolution modeling of western Alaskan tides and storm surge under
791 varying sea ice conditions, *Ocean Modelling*, 141, 101421,
792 <https://doi.org/10.1016/j.ocemod.2019.101421>, 2019.
- 793 Kalnay, E., Kanamitsu, M., Kistler, R., Collins, W., Deaven, D., Gandin, L., Iredell, M., Saha, S.,
794 White, G., Woollen, J., Zhu, Y., Chelliah, M., Ebisuzaki, W., Higgins, W., Janowiak, J., Mo, K.
795 C., Ropelewski, C., Wang, J., Leetmaa, A., Reynolds, R., Jenne, R., and Joseph D.: The
796 NCEP/NCAR 40-year reanalysis project, *Bull. Am. Meteorol. Soc.*, 77, 437–471,
797 [https://doi.org/10.1175/1520-0477\(1996\)077<0437: TNYRP>2.0.CO;2](https://doi.org/10.1175/1520-0477(1996)077<0437: TNYRP>2.0.CO;2), 1996.
- 798 Kuzyk, Z. A., Macdonald, R.W., Stern, G. A., and Gobeil, C.: Inferences about the modern
799 organic carbon cycle from diagenesis of redox-sensitive elements in Hudson Bay, *Journal of*
800 *Marine Systems*, 88, 451–462, <https://doi.org/10.1016/j.jmarsys.2010.11.001>, 2011.
- 801 Kuzyk, Z. A. and Candlish, L. M.: From Science to Policy in the Greater Hudson Bay Marine
802 Region: An Integrated Regional Impact Study (IRIS) of Climate Change and Modernization,
803 ArcticNet, Québec City, 424 pp, 2019
- 804 Landy, J. C., Ehn, J. K., Babb, D. G., Theriault, N., and Barber, D. G.: Sea ice thickness in the
805 eastern Canadian Arctic: Hudson Bay complex & Baffin Bay, *Remote Sensing of Environment*,
806 200, 281–294, <https://doi.org/10.1016/j.rse.2017.08.019>, 2017.
- 807 Larson, K. M., and van Dam, T.: Measuring postglacial rebound with GPS and absolute gravity,
808 *Geophys. Res. Lett.*, 27, 3925–3928, <https://doi.org/10.1029/2000GL011946>, 2000.
- 809 [Lüpkes, C., Gryanik, V. M., Hartmann, J., and Andreas, E. L.: A parametrization, based on sea](#)
810 [ice morphology, of the neutral atmospheric drag coefficients for weather prediction and climate](#)
811 [models, *J. Geophys. Res. Atmospheres*, 117, D13112, <https://doi.org/10.1029/2012JD017630>,](#)
812 [2012.](#)
- 813 Mulet, S., Rio, M. H., Greiner, E., Picot, N., and Pascual, A.: New global Mean Dynamic
814 Topography from a GOCE geoid model, altimeter measurements and oceanographic in-situ data,
815 OSTST Boulder, USA, available at:
816 http://www.aviso.altimetry.fr/fileadmin/documents/OSTST/2013/oral/mulet_MDT_CNES_CLS
817 [13.pdf, 2013, last access: 26 August 2021.](#)
- 818 Pascual, A., Boone, C., Larnicol, G., and Le Traon, P.-Y.: On the quality of real-time altimeter
819 gridded fields: Comparison with in situ data, *J. Atmos. Oceanic Technol.*, 26, 556–569,
820 <https://doi.org/10.1175/2008JTECHO556.1>, 2009.
- 821 Piecuch, C. G., and Ponte, R. M.: A wind-driven nonseasonal barotropic fluctuation of the
822 Canadian inland seas, *Ocean Sci.*, 11, 175–185, <https://doi.org/10.5194/os-11-175-2015>, 2015.
- 823 Piecuch, C. G., and Ponte, R. M.: Nonseasonal mass fluctuations in the midlatitude North
824 Atlantic Ocean, *Geophys. Res. Lett.*, 41, 4261–4269, <https://doi.org/10.1002/2014GL060248>,
825 2014.

- 826 Prinsenberg, S. J.: Freshwater contents and heat budgets of James Bay and Hudson Bay,
827 *Continental Shelf Res.*, 3(2), 191-200, [https://doi.org/10.1016/0278-4343\(84\)90007-4](https://doi.org/10.1016/0278-4343(84)90007-4), 1984.
- 828 Prinsenberg, S. J.: Salinity and temperature distribution of Hudson Bay and James Bay, In:
829 Martini, E. P. (ed.) *Canadian Inland Seas*, Oceanogr. Ser. 44, Elsevier, New York, pp 163–186,
830 1986a.
- 831 Prinsenberg, S. J.: The circulation pattern and current structure of Hudson. In: Martini, E. P. (ed.)
832 *Canadian Inland Seas*, Oceanogr. Ser. 44, Elsevier, New York, 187–203, 1986b.
- 833 Prinsenberg, S. J.: Ice-cover and ice-ridge contributions to the freshwater contents of Hudson
834 Bay and Foxe Basin, *Arctic*, 41(1), 6–11, <https://doi.org/10.14430/arctic1686>, 1988.
- 835 Prinsenberg, S. J.: Effects of hydro-electric projects on Hudson Bay's marine and ice
836 environments, *Potential Environ. Impacts Ser. 2*, 8 pp., North Wind Inf. Serv., Montreal, 1991.
- 837 Pujol, M.-I., Faugère, Y., Taburet, G., Dupuy, S., Pelloquin, C., Ablain, M., and Picot, N.:
838 DUACS DT2014: the new multi-mission altimeter data set reprocessed over 20 years, *Ocean*
839 *Sci.*, 12, 1067-1090, <https://doi.org/0.5194/os-12-1067-2016>, 2016.
- 840 Pew Charitable Trusts: The Integrated Arctic Corridors Framework. Planning for responsible
841 shipping in Canada's Arctic waters, available at:
842 [https://www.pewtrusts.org/~media/Assets/2016/04/The-Integrated-Arctic-Corridors-](https://www.pewtrusts.org/~media/Assets/2016/04/The-Integrated-Arctic-Corridors-Framework.pdf)
843 [Framework.pdf](https://www.pewtrusts.org/~media/Assets/2016/04/The-Integrated-Arctic-Corridors-Framework.pdf), 2016, last access: 26 August 2021.
- 844 Ray, R. D.: Sea Level, Land Motion, and the Anomalous Tide at Churchill, Hudson Bay,
845 *American Geophysical Union, Fall Meeting 2015*, abstract id. G43B-1040, 2015.
- 846 Ridenour, N. A., Hu, X., Sydor, K., Myers, P. G., and Barber, D. G.: Revisiting the circulation of
847 Hudson Bay: Evidence for a seasonal pattern, *Geophysical Research Letters*, 46, 3891–3899,
848 <https://doi.org/10.1029/2019GL082344>, 2019a.
- 849 Ridenour, N. A., Hu, X., Jafarikhasragh, S., Landy, J. C., Lukovich, J. V., Stadnyk, T. A., Sydor,
850 K., Myers, P. G., and Barber, D. G.: Sensitivity of freshwater dynamics to ocean model
851 resolution and river discharge forcing in the Hudson Bay Complex, *Journal of Marine Systems*,
852 196, 48-64, <https://doi.org/10.1016/j.jmarsys.2019.04.002>, 2019b.
- 853 Sella, G. F., Stein, S., Dixon, T. H., Craymer, M., James, T. S., Mazzotti, S., and Dokka, R. K.:
854 Observation of glacial isostatic adjustment in “stable” North America with GPS, *Geophys. Res.*
855 *Lett.*, 34, L02306, <https://doi.org/10.1029/2006GL027081>, 2007.
- 856 Smith, C. A., Compo, G. P., and Hooper, D. K.: Web-based reanalysis intercomparison tools
857 (WRIT) for analysis and comparison of reanalyses and other datasets, *Bull. Amer. Meteor. Soc.*,
858 95(11): 1671–1678, <https://doi.org/10.1175/BAMS-D-13-00192.1>, 2014.
- 859 Saucier, F. J., and Dionne, J.: A 3-D coupled ice-ocean model applied to Hudson Bay, Canada:
860 The seasonal cycle and time-dependent climate response to atmospheric forcing and runoff, *J.*
861 *Geophys. Res. Oceans*, 103(C12), 27,689-27,705, <https://doi.org/10.1029/98JC02066>, 1998.

- 862 Saucier, F. J., Senneville, S., Prinsenber, S., Roy, F., Smith, G., Gachon, P., Caya, D., and
863 Laprise, R.: Modelling the sea ice-ocean seasonal cycle in Hudson Bay, Foxe Basin and Hudson
864 Strait, Canada, *Climate Dynamics*, 23, 303–326, <https://doi.org/10.1007/s00382-004-0445-6>,
865 2004.
- 866 [Schulze, L. M. and Pickart, R. S.: Seasonal variation of upwelling in the Alaskan Beaufort Sea:
867 Impact of sea ice cover, *J. Geophys. Res.*, 117, C06022, <https://doi.org/10.1029/2012JC007985>,
868 2012.](#)
- 869 St-Laurent, P., Straneo, F., Dumais, J.-F., and Barber, D. G.: What is the fate of the river waters
870 of Hudson Bay?, *Journal of Marine Systems*, 88, 352–361,
871 <https://doi.org/10.1016/j.jmarsys.2011.02.004>, 2011.
- 872 Straneo, F., and Saucier, F.: The outflow from Hudson Strait and its contribution to the Labrador
873 Current, *Deep-Sea Res. I*, 55, 926–946, <https://doi.org/10.1016/j.dsr.2008.03.012>, 2008.
- 874 [The Climate Change Initiative Coastal Sea Level Team. Coastal sea level anomalies and
875 associated trends from Jason satellite altimetry over 2002–2018: *Sci. Data*, 7, 357,
876 <https://doi.org/10.1038/s41597-020-00694-w>, 2020.](#)
- 877 Tivy, A., Howell, S. E., Alt, B., Yackel, J. J., and Carrieres, T.: Origins and levels of seasonal
878 forecast skill for sea ice in Hudson Bay using Canonical Correlation Analysis, *J. Climate*, 24(5),
879 1378–1395, <https://doi.org/10.1175/2010JCLI3527.1>, 2011.
- 880 [Tsamados, M., Feltham, D. L., Schroeder, D., Flocco, D., Farrell, S. L., Kurtz, N., Laxon, S. W.,
881 and Bacon, S.: Impact of Variable Atmospheric and Oceanic Form Drag on Simulations of
882 Arctic Sea Ice, *J. Phys. Oceanography*, 44\(5\), 1329–1353, \[https://doi.org/10.1175/JPO-D-13-
0215.1\]\(https://doi.org/10.1175/JPO-D-13-
883 0215.1\), 2014.](#)
- 884 Tushingam, A. M.: Observations of postglacial uplift at Churchill, Manitoba, *Canadian Journal
885 of Earth Sciences*, 29, 2418–2425, <https://doi.org/10.1139/e92-189>, 1992.
- 886 [Volkov, D. L., and Pujol, M.-I.: Quality assessment of a satellite altimetry data product in the
887 Nordic, Barents, and Kara seas, *J. Geophys. Res.*, 117, C03025,
888 <https://doi.org/10.1029/2011JC007557>, 2012.](#)
- 889 [Volkov, D. L., Larnicol, G., and Dorandeu, J.: Improving the quality of satellite altimetry data
890 over continental shelves, *J. Geophys. Res.*, 112, C06020, <https://doi.org/10.1029/2006JC003765>,
891 2007.](#)
- 892 Ward, P. J., Couasnon, A., Eilander, D., Haigh, I. D., Hendry, A., Muis, S., Veldkamp, T. I. E.,
893 Winsemius, H. C., and Wahl, T.: Dependence between high sea-level and high river discharge
894 increases flood hazard in global deltas and estuaries, *Environ. Res. Lett.*, 13, 084012,
895 <https://doi.org/10.1088/1748-9326/aad400>, 2018.
- 896 Walsh, J. E., Chapman, W. L., and Shy, T. L.: Recent decrease of sea level pressure in the
897 central Arctic, *J. Clim.*, 9, 480–486, [https://doi.org/10.1175/1520-0442\(1996\)009<0480:
898 RDOSLP>2.0.CO;2](https://doi.org/10.1175/1520-0442(1996)009<0480:RDOSLP>2.0.CO;2), 1996.

899 Wang, J., L. Mysak, A. and Ingram, R. G.: A Three-Dimensional Numerical Simulation of
900 Hudson Bay Summer Ocean Circulation: Topographic Gyres, Separations, and Coastal Jets, *J.*
901 *Phys. Oceanogr.*, 24, 2496–2514, [https://doi.org/10.1175/1520-](https://doi.org/10.1175/1520-0485(1994)024<2496:ATDNSO>2.0.CO;2)
902 0485(1994)024<2496:ATDNSO>2.0.CO;2, 1994.

903 Wolf, D., Klemann, V. and Wunsch, J.: A Reanalysis and Reinterpretation of Geodetic and
904 Geological Evidence of Glacial-Isostatic Adjustment in the Churchill Region, Hudson Bay, *Surv.*
905 *Geophys.*, 27, 19–61, <https://doi.org/0.1007/s10712-005-0641-x>, 2006.

906 **Tables**

907 **Table 1:** Correlations (R) of daily atmospheric vorticity and/or Churchill River discharge and sea
 908 level anomalies in western Hudson Bay for the whole annual cycle

Predictor(s)/Time frame	1960 - 2019	Pre-diversion 1960 - 1976	Post-diversion 1977 - 2019
Vorticity	0.47	0.49	0.47
River discharge	0.22	0.20	0.23
Vorticity and river discharge*	0.53*	0.53*	0.53*

909

910 **Table 2:** Correlations (R) of monthly-mean atmospheric vorticity and/or Churchill River
 911 discharge and sea level anomalies in western Hudson Bay for the ice-free period (June-
 912 November)

Predictor(s)/Time frame	1960 - 2019	Pre-diversion 1960 - 1976	Post-diversion 1977 - 2019
Vorticity	0.54	0.52	0.55
River discharge	0.08	0.03**	0.11
Vorticity and river discharge*	0.55*	0.52*	0.57*

913

914 **Table 3:** Correlations (R) of monthly-mean atmospheric vorticity and/or Churchill River
 915 discharge and sea level anomalies in western Hudson Bay for the ice-covered period (December-
 916 May)

Predictor(s)/Time frame	1960 - 2019	Pre-diversion 1960 - 1976	Post-diversion 1977 - 2019
Vorticity	0.47	0.49	0.47
River discharge	0.21	0.12	0.19
Vorticity and river discharge*	0.52*	0.51*	0.52*

917

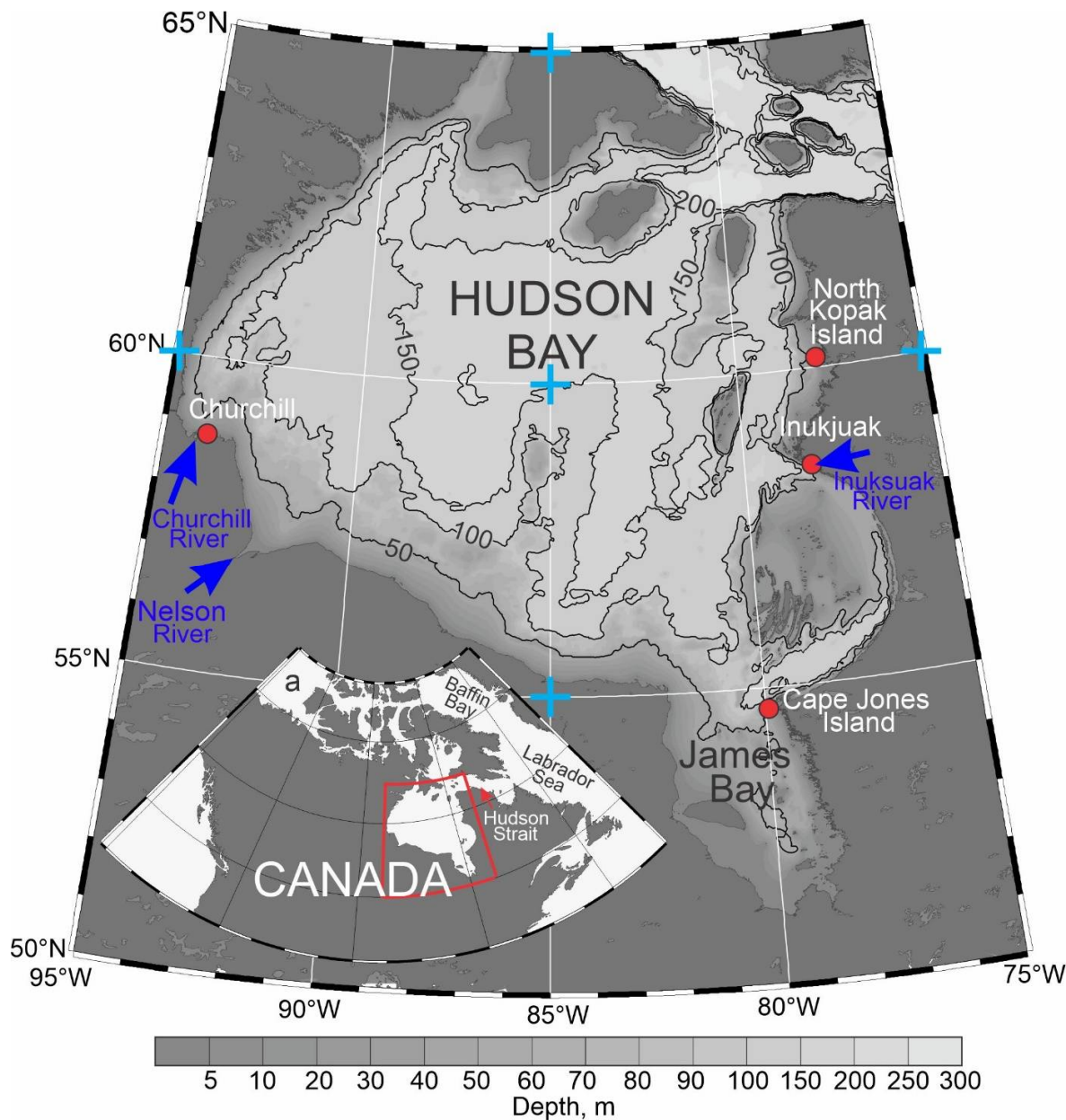
918 *The coefficient of multiple correlation is estimated based on the multiple linear regression
 919 analysis

920 ** Correlation not statistically significant at the 99% confidence level

921 **Figures**

922

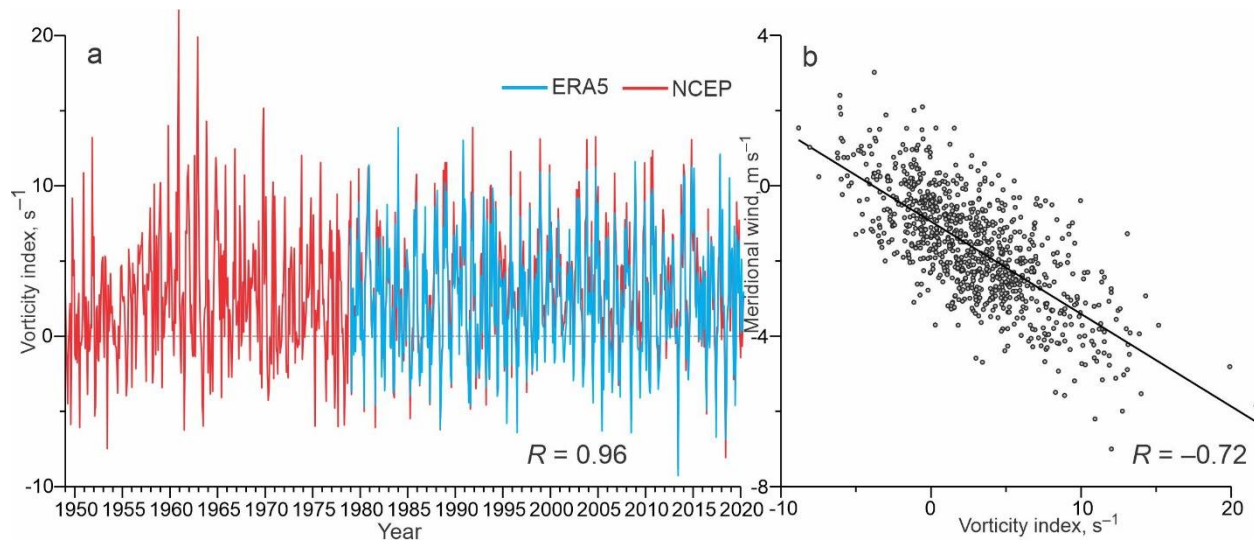
923



924

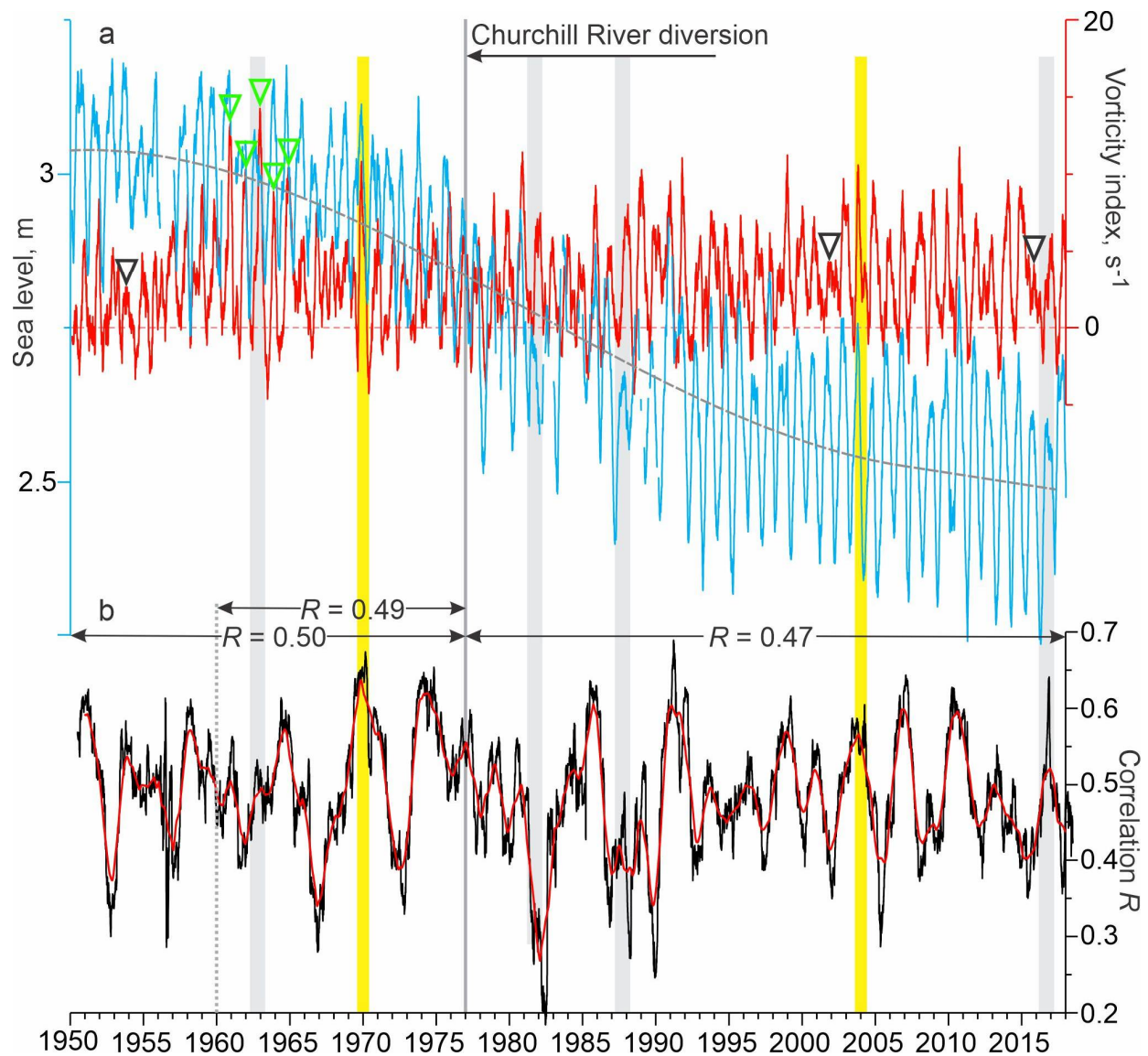
925 **Figure 1:** Map of Hudson Bay. Red dots depict the permanent tide gauge in Churchill and
 926 temporary tide gauges in Inukjuak, Cape Jones Island and North Kopak Island. Blue arrows
 927 highlight Churchill, Nelson and Inuksuak river mouths. Blue crosses depict the 5-point stencil
 928 used for computing atmospheric vorticity approximated as Laplacian from sea level atmospheric
 929 pressure. The numbered black lines depict depth contours of 50, 100, 150 and 200 m. (a) Inset
 930 shows the Hudson Bay location within North America. The map of Hudson Bay was compiled
 931 based on the General Bathymetric Chart of the Oceans (GEBCO, www.gebco.net).

932
933
934
935
936
937



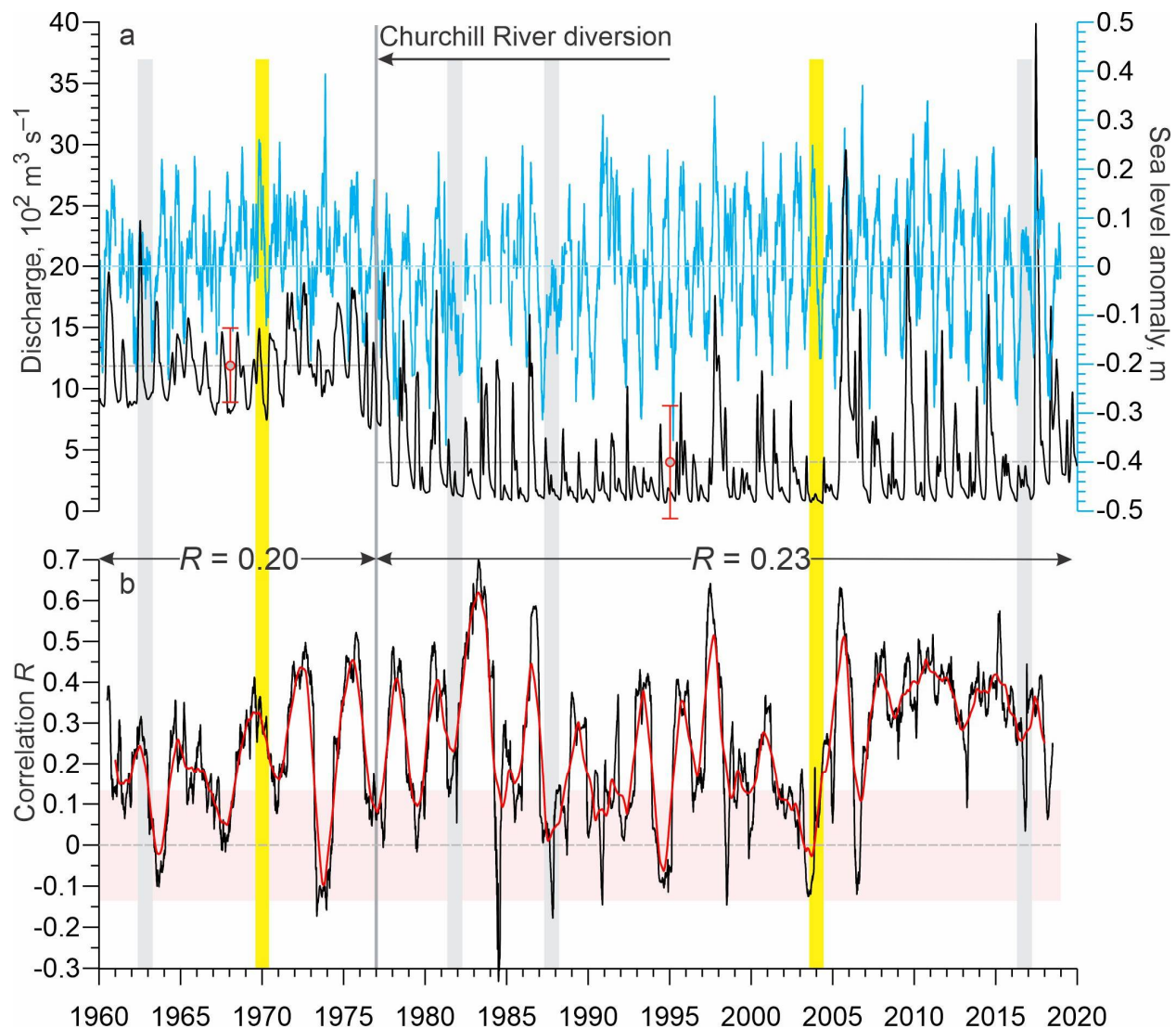
938
939
940
941
942
943
944
945
946

Figure 2: (a) Time series of the monthly mean atmospheric vorticity index (s^{-1}) over Hudson Bay, derived from NCEP (red) and ERA5 (blue). (b) Scatter plot of the monthly mean meridional wind seaward of Churchill in western Hudson Bay ($m s^{-1}$) versus the monthly mean atmospheric vorticity index. Thick black line depicts linear regression. Numbers at the bottom show correlation R between (a) the monthly mean vorticity derived from NCEP (1949-2000) and ERA5 (1979-2000) and (b) the monthly mean NCEP vorticity versus meridional wind (1949-2020).



947
 948 **Figure 3:** (a) 91-day running mean of daily mean atmospheric vorticity index (red, s⁻¹) over
 949 Hudson Bay and daily-mean sea level measured at the tide gauge in Churchill (blue, m). Positive
 950 and negative vorticity correspond to cyclonic and anticyclonic atmospheric circulation,
 951 respectively. Gray dashed line shows polynomial approximation of the sea level trend attributed
 952 to the glacial isostatic adjustment. Black and green triangles show periods when seasonal
 953 vorticity from late fall to early winter was diminished and amplified, respectively. (b)
 954 Correlation R between daily vorticity index and sea level anomaly (SLA) computed for the 365-
 955 day moving window (black) with their 365-day running mean (red). All correlations are
 956 statistically significant at 99% confidence. Numbers at the top show correlation between daily
 957 vorticity index and SLA computed for 1950/60-1976 and 1977-2018 pre- and post-diversion,
 958 respectively. (a, b) Yellow shading highlights August-May 1969-70 and 2003-04, enlarged in
 959 Figure 6. Black arrow indicates onset of the Churchill River diversion. Gray shading highlights
 960 periods when the sea level seasonal cycle was partially disrupted (1981-82 and 1987-88), or
 961 significantly diminished (1962-63 and 2016-2017).

962

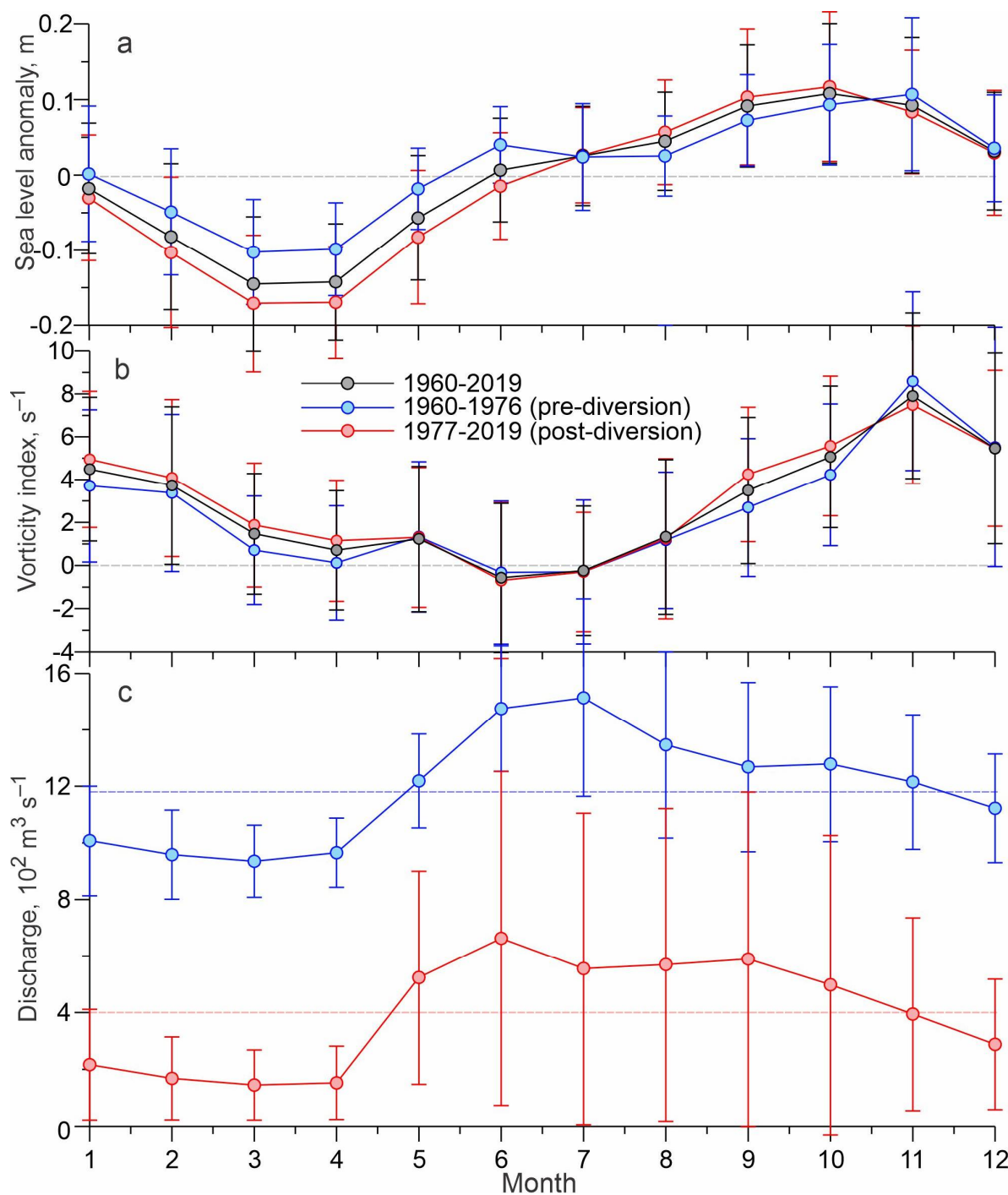


963

964

965 **Figure 4:** (a) 30-day running mean of the Churchill River discharge (black; $10^2 \text{ m}^3 \text{ s}^{-1}$) and
 966 detrended ~~daily-mean~~ SLA at Churchill (blue; m). Gray circles show mean discharge pre- and
 967 post-diversion with standard deviations depicted with red error bars. (b) Correlation R between
 968 daily Churchill River discharge and SLA computed for the 365-day moving window (black) with
 969 their 365-day running mean (red). Pink shading highlights statistically insignificant correlations
 970 at the 99% confidence level. Numbers at the top show correlation between daily Churchill River
 971 discharge and SLA computed for 1950-1976 and 1977-2018 pre- and post-diversion,
 972 respectively. (a, b) Yellow shading highlights August-May 1969-70 and 2003-04. Black arrow
 973 indicates onset of the Churchill River diversion. Gray shading highlights periods when the sea
 974 level seasonal cycle was partially disrupted (1981-82 and 1987-88), or significantly diminished
 975 (1962-63 and 2016-2017).

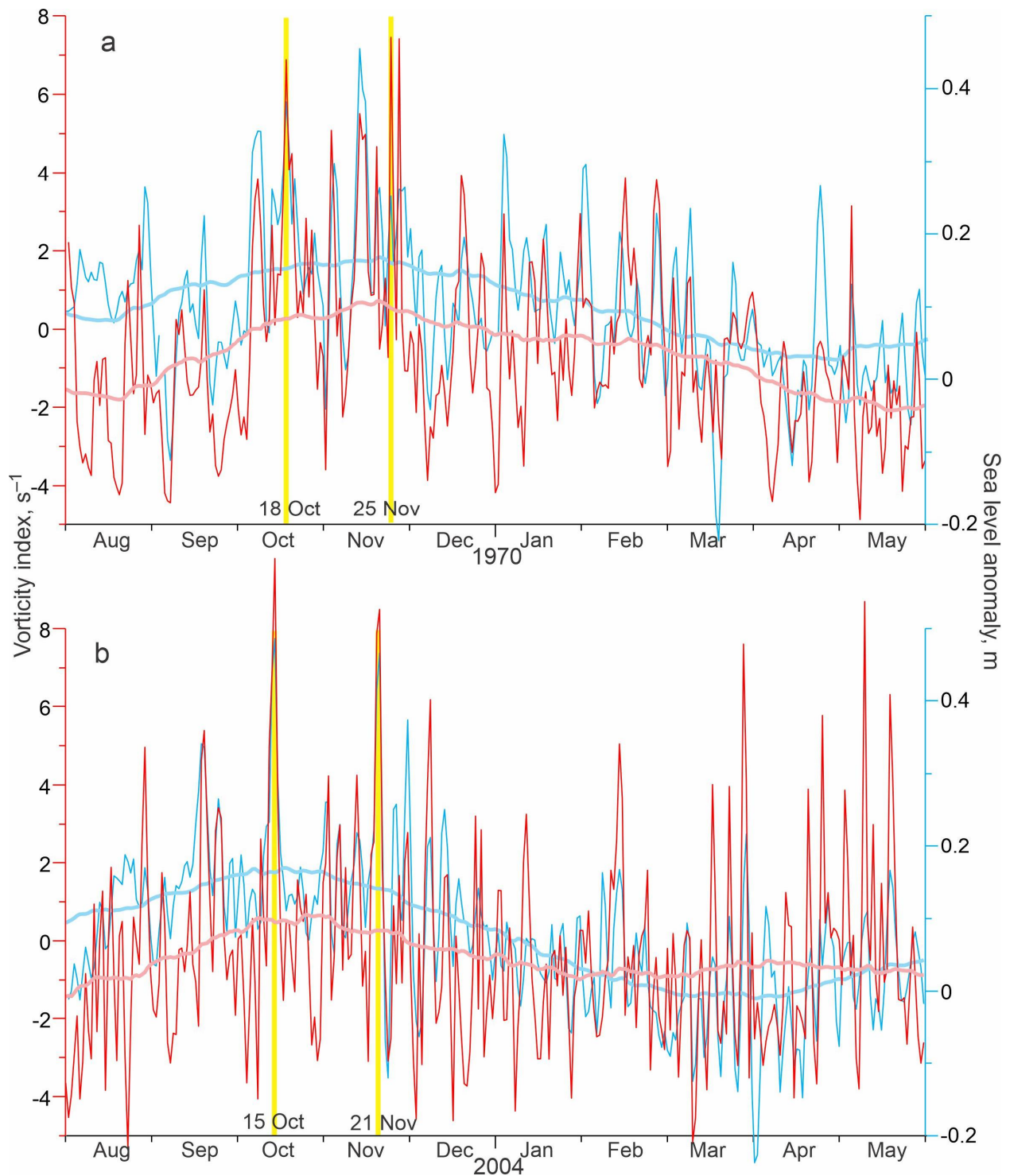
976



977

978 **Figure 5:** Seasonal cycle of (a) SLA at Churchill (m), (b) atmospheric vorticity over Hudson
 979 Bay (s^{-1}), and (c) Churchill River discharge ($10^2 m^3 s^{-1}$). Seasonal cycle derived using monthly-
 980 mean data for (a, b) 1950-2019 (black), (a, b) 1950-76 (blue) and (c) 1960-76 (blue) before the
 981 Churchill River diversion, and (a, b, c) 1977-2018 (red) after the Churchill River diversion. Error
 982 bars show \pm one standard deviation of the mean. (c) Blue and pink dashed lines show the long-
 983 term mean discharge before and after diversion, respectively.

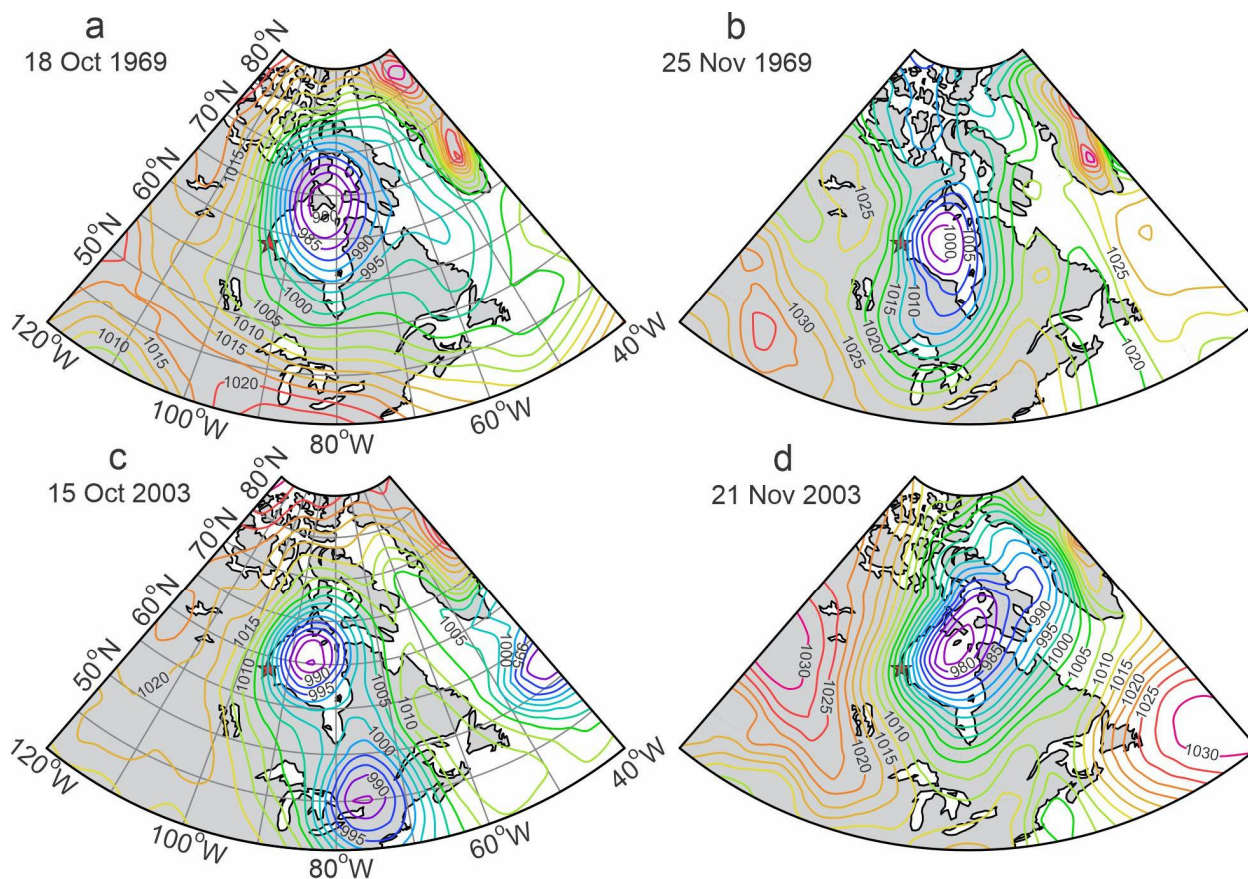
984



985

986 **Figure 6:** Time series of the daily mean vorticity index (red; s⁻¹) and SLA at Churchill (blue; m)
 987 with their 91-day running mean in pink and light blue, respectively, for August/May (a)
 988 1969/1970 and (b) 2003/2004. (a, b) Vertical yellow lines highlight coherent peaks in vorticity
 989 and sea level in October and November.

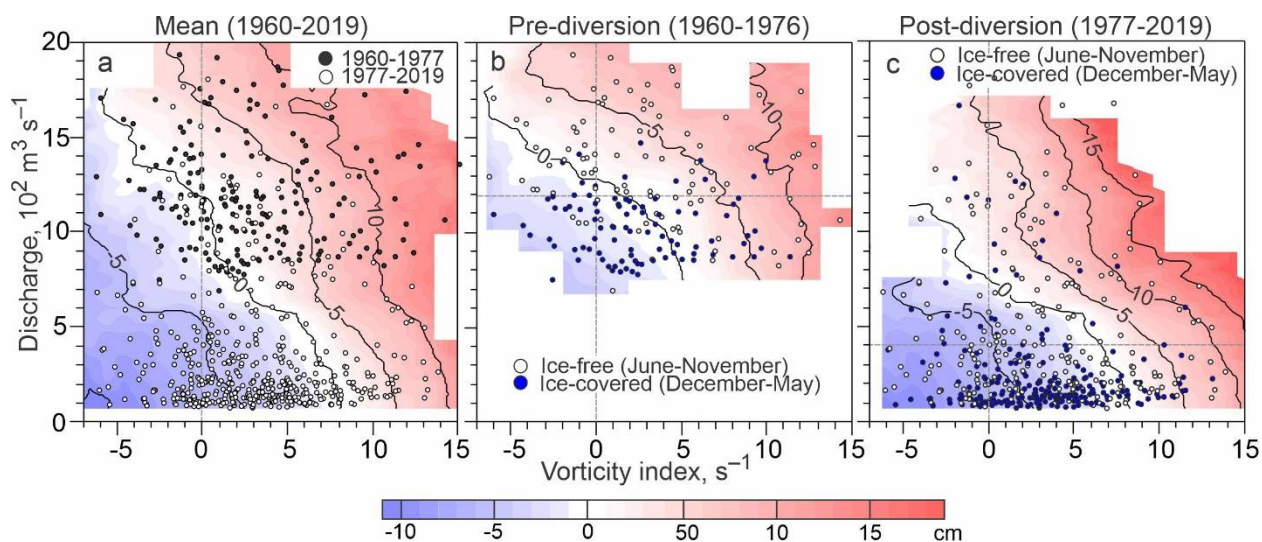
990
991
992
993
994



995
996
997
998
999

Figure 7: Sea level atmospheric pressure (hPa) for coherent peaks in atmospheric vorticity and sea level at Churchill, highlighted in Figure 6 with yellow lines: (a) 18 October 1969, (b) 25 November 1969, (c) 15 October 2003, and (d) 21 November 2003.

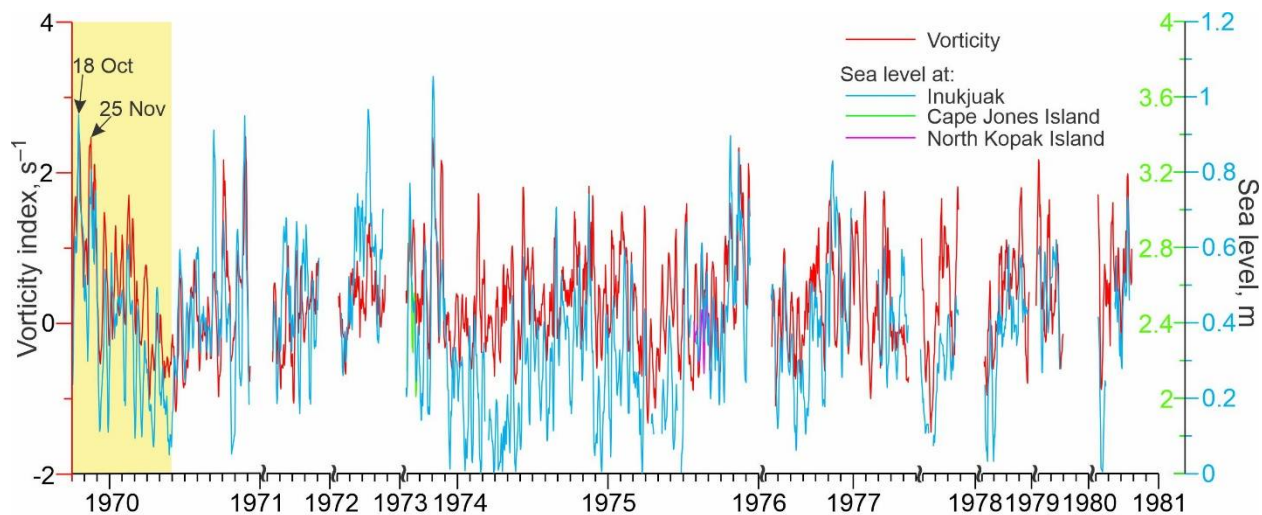
1000
1001
1002
1003
1004
1005
1006



1007
1008
1009
1010
1011
1012
1013
1014
1015
1016
1017

Figure 8: Color shading shows monthly mean sea level anomalies (cm) from tidal gauge at Churchill versus atmospheric vorticity (s^{-1} ; horizontal axis) and Churchill River discharge ($10^2 m^3 s^{-1}$; vertical axis) for (a) entire period of river discharge observations (1960 – 2019), and (b) before and (c) after the Churchill River diversion in 1977. Scatter plots show monthly mean vorticity and river discharge for (a) 1960-1976 (black circles) and 1977-2019 (white circles), and (b, c) ice-free season (June-November; white circles) and ice-covered season (December-May; blue circles). Horizontal gray dashed line shows mean river discharge (c) before and (d) after diversion.

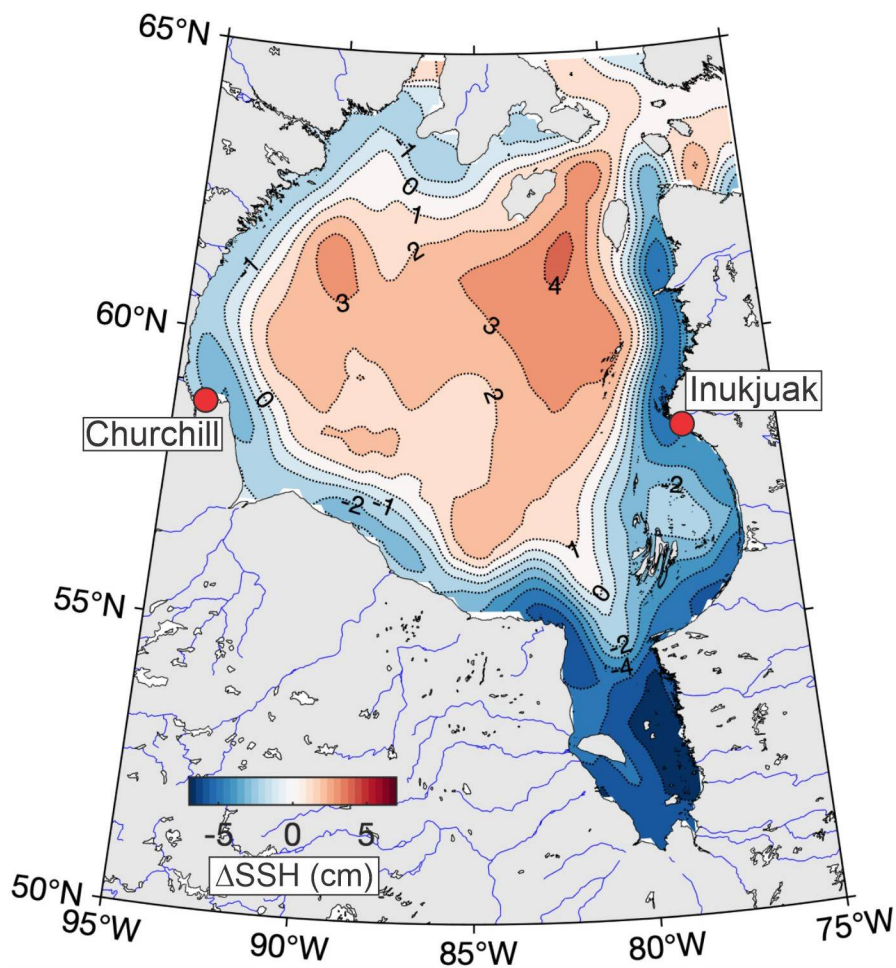
1018
1019
1020
1021
1022
1023



1024
1025
1026
1027
1028
1029
1030
1031

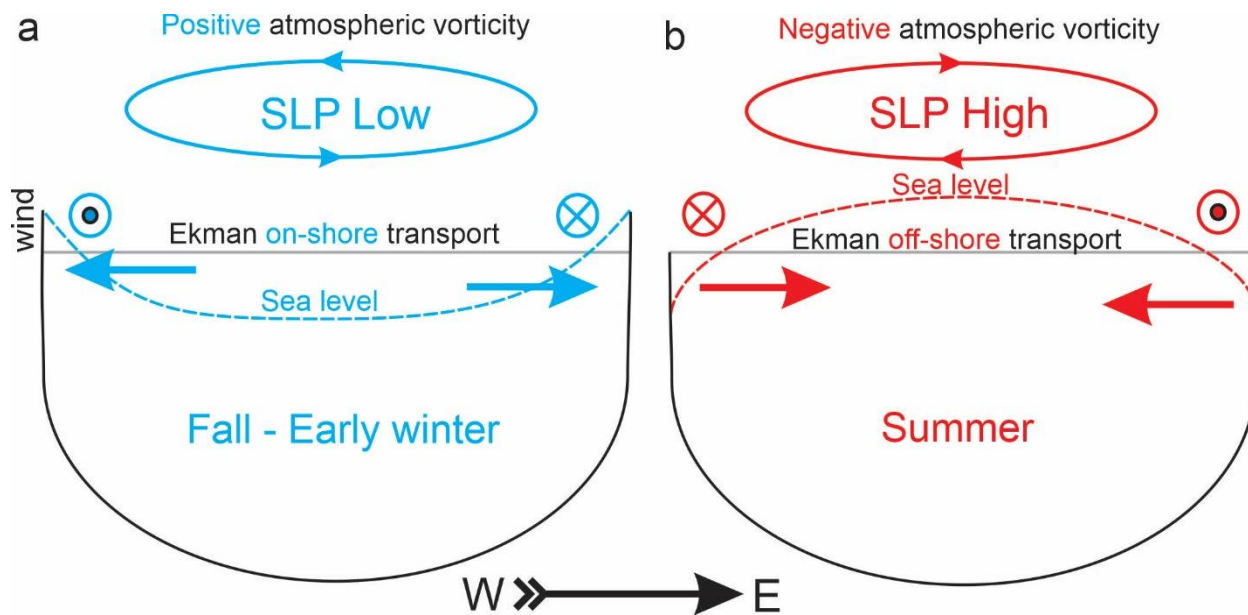
Figure 9: Time series of 7-day running mean for daily atmospheric vorticity index (red, s^{-1}) over Hudson Bay and daily mean sea level (m) measured at the tide gauge in Inukjuak (blue), Cape Jones Island (green) and North Kopak Island (purple). Yellow shading highlights October/May 1969/70. Black arrows indicate two cyclonic storms in 18 October and 25 November 1969 with atmospheric forcing shown in Figures 7a and 7b, respectively. Right vertical axis shows sea-level scale for Inukjuak (blue), and Cape Jones Island and North Kopak Island (green).

1032
1033
1034
1035



1036
1037 **Figure 10:** The long-term mean (1993-2020) difference between sea surface height (SSH; cm) in
1038 summer (June-August) and fall (September-November) derived from the satellite altimetry. Red
1039 dots depict the tide gauge in Churchill and Innukjuak.
1040

1041
1042
1043
1044
1045
1046



1047
1048
1049
1050
1051
1052
1053
1054
1055

Figure 11: Diagram of the proposed impact of the seasonal changes in atmospheric vorticity on the sea level seasonal variability in Hudson Bay. (a) Positive (cyclonic) vorticity during October-December causes onshore Ekman transport and storm surges over the coast. (b) Negative (anticyclonic) vorticity during June-July forces offshore Ekman transport. During winter, a complete sea-ice cover reduces momentum transfer from wind stress to the water column diminishing impact of atmospheric forcing on sea level variability. Dotted and crossed circles depict southerly and northerly along-shore surface winds, respectively.